Mon. Not. R. Astron. Soc. **000**, 1–14 () Printed 8 October 2014 (MN LATEX style file v2.2)

A deep catalogue of classical Be stars in the direction of the Perseus Arm: spectral types and interstellar reddenings.

R. Raddi[1,2⋆], J. E. Drew[1], D. Steeghs[2], N. J. Wright[1], J. J. Drake[3], G. Barentsen[1], J. Fabregat[4], S. E. Sale[5]

[1]*Centre for Astrophysics Research, STRI, University of Hertfordshire, College Lane Campus, Hatfield, AL10 9AB, U.K.*
[2]*Department of Physics, University of Warwick, Gibbet Hill Road, Coventry, CV4 7AL, U.K.*
[3]*Smithsonian Astrophysical Observatory, 60 Garden Street, Cambridge, MA 02138, USA*
[4]*Observatorio Astronómico, Universidad de Valencia, 46100 Burjassot, Spain*
[5]*Rudolf Peierls Centre for Theoretical Physics, Keble Road, Oxford OX1 3NP, UK*

Accepted 2014 October 05. Received 2014 October 05; in original form 2014 June 30

ABSTRACT

We present a catalogue of 247 photometrically and spectroscopically confirmed fainter classical Be stars ($13 \lesssim r \lesssim 16$) in the direction of the Perseus Arm of the Milky Way ($-1^\circ < b < +4^\circ$, $120^\circ < \ell < 140^\circ$). The catalogue consists of 181 IPHAS-selected new classical Be stars, in addition to 66 objects that were studied by Raddi et al. (2013) more closely, and 3 stars identified as classical Be stars in earlier work. This study more than doubles the number known in the region. Photometry spanning 0.6 to 5 μm, spectral types, and interstellar reddenings are given for each object. The spectral types were determined from low-resolution spectra (λ / $\Delta\lambda \approx$ 800–2000), to a precision of 1–3 subtypes. The interstellar reddenings are derived from the $(r-i)$ colour, using a method that corrects for circumstellar disc emission. The colour excesses obtained range from $E(B-V) = 0.3$ up to 1.6 – a distribution that modestly extends the range reported in the literature for Perseus-Arm open clusters. For around half the sample, the reddenings obtained are compatible with measures of the total sightline Galactic extinction. Many of these are likely to lie well beyond the Perseus Arm.

Key words: stars: emission-line, early-type, Be - ISM: dust, extinction, structure

1 INTRODUCTION

The first classical Be star to be classified was γCas, identified by Father Angelo Secchi almost 150 years ago. Secchi described it as showing a particularly curious bright line – in that case, Hβ – as opposed to the dark lines observed in the spectra of stars with similar colours (Secchi 1866). Presently, the family of classical Be stars numbers over 2000 known members in the all-sky Be Star Spectra database (BeSS[1], Neiner et al. 2011).

Following the original definition given by Collins (1987), classical Be stars are non-supergiant early-type stars whose spectra have, or have had at some time, one or more Balmer lines in emission (Porter & Rivinius 2003). They do not present forbidden emission lines in their spectra. They are also characterised by excess continuum emission at ultraviolet (UV), optical, and infrared (IR) wavelengths (e.g. see Dachs, Kiehling & Engels 1988, Kaiser 1989; Zorec & Briot 1991; Dougherty et al. 1994). The presence of dense and hot ($n_e \approx 10^{12}$ cm^{-3}, $T_e \approx 10000$ K) circumstellar decretion discs is the cause of the observed free-free and free-bound optically-thin continuum emission, and also the line emission (Gehrz, Hackwell & Jones 1974, Dachs et al. 1988; Carciofi & Bjorkman 2006). The continuum excess emission has been carefully characterised in the past, in order to understand its origins and to separate out its contribution to observed optical and IR fluxes (Dachs et al. 1988; Zorec & Briot 1991; Dougherty et al. 1994). Fast rotation is specially brought up as one of the main factors behind the formation of the circumstellar discs (Townsend et al. 2004; Cranmer 2005). Carciofi et al. (2012) have provided evidence that the circumstellar disc of classical Be stars approximates a viscous decretion disc as described by Lee, Osaki & Saio (1991). Evidence for Keplerian rotation of the disc matter around the B star has been obtained by Meilland et al. (2007) and Oudmaijer et al. (2011). More recently still, the requirement of a fast-rotating B-type stars has been added to the definition of classical Be star (Rivinius, Carciofi & Martayan 2013).

In the past, there has been some debate regarding the evolutionary status of classical Be stars (Mermilliod 1982; Slettebak 1985; Fabregat & Torrejón 2000). More recently the controversy has started to settle. Martayan et al. (2007) found, through studying classical Be stars both in the Milky Way and in the Magel-

⋆ E-mail: r.raddi@warwick.ac.uk
[1] http://basebe.obspm.fr

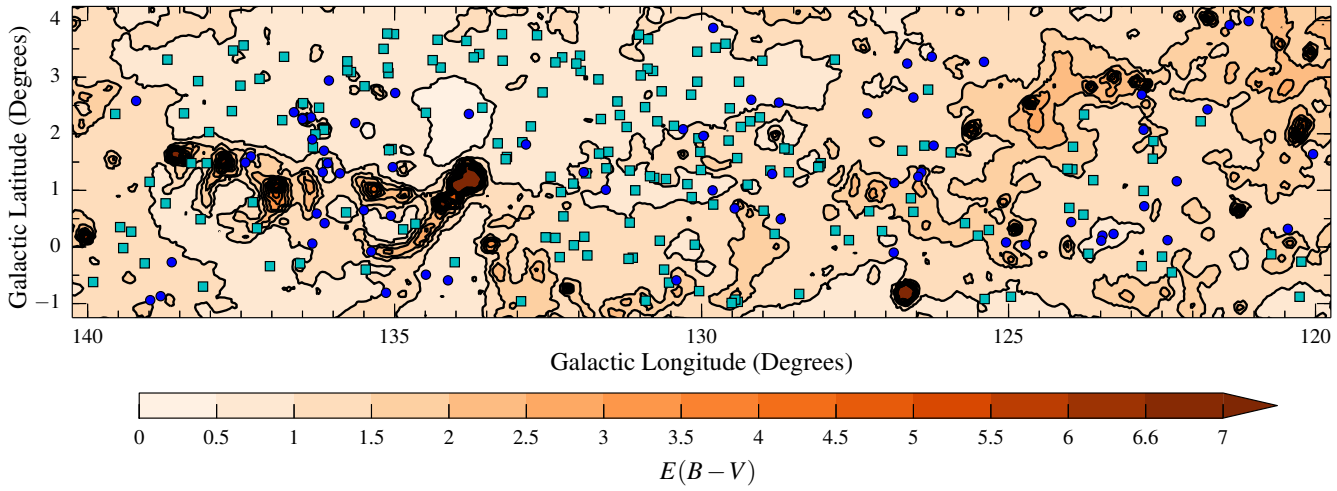

Figure 1. The spatial distribution on the sky of the studied classical Be stars is plotted on the map of the interstellar dust extinction computed by SFD98. We applied the correction ($0.86 \times E(B-V)$) suggested by Schlafly et al. (2010) to the SFD98 maps, colour coding the levels of extinction that are binned in 0.5 mag steps and cut at $E(B-V) = 7$ – with the lightest colour mapping the 0–0.5 mag range. The cyan squares symbols denote the 181 classical Be stars observed with FLWO-1.5m/FAST, while the blue circles represent the 67 classical Be stars observed in La Palma. We note that the minimum SFD98 is measured above the W4 H II bubble ($\ell \approx 134$, $b \approx 2.5$), where $E(B-V) \sim 0.3$, corresponding to the first reddening bin of the colour-scale. The most obscured regions with $E(B-V) > 7$ correspond to the densest areas of the Perseus arm, where ongoing star formation is observed (specially W3/W4/W5 and Cas OB 7).

lanic Clouds, that the evolution of the rotation speeds with age is mass and metallicity dependent. This work concluded that the Be phenomenon, in our Galaxy, appears earlier in the main sequence (MS) life at higher stellar masses ($\sim 12\,M_{\odot}$) and earlier spectral types, while it is delayed in lower mass stars ($\sim 5\,M_{\odot}$), or equivalently, in later B-types, confirming previous observations of classical Be stars in open clusters (Fabregat & Torrejón 2000). In general, classical Be stars can be viewed as relatively (but not very) young stars that are typically observed in open clusters up to 100 Myr old, with highest incidence in clusters with ages in the range of 13–25 Myr, which are typical of the turn-off age of B2 stars (Fabregat & Torrejón 2000). On the other hand, observations of Galactic-field bright classical Be stars show a flat distribution across the B subtypes (Zorec & Briot 1997), which could be explained by the relatively smaller numbers of known old open clusters (e.g. in Dias et al. 2002) and high "infant-mortality" (see e.g. Goodwin & Bastian 2006).

In Raddi et al. (2013, hereafter paper I), we studied a sample of 67 classical Be stars, located within a section of the Galactic plane between $120^{\circ} \leqslant \ell \leqslant 140^{\circ}$ and $-1^{\circ} \leqslant b \leqslant +4^{\circ}$ for which intermediate-dispersion optical spectra were available. Our stars were picked out from a larger set of candidate emission line stars selected photometrically from the Isaac Newton Telescope (INT) Photometric Hα Survey of the Northern Galactic Plane (IPHAS, Drew et al. 2005). In paper I, we investigated whether the dereddened sample could provide any hints of spiral arm structure in this section of the thin disc, but concluded that the errors in the spectroscopic parallaxes wash out any distinction between a smooth or spiral-arm dominated stellar density profile. Nevertheless, the study represented a step change to a sample of classical Be stars that is appreciably fainter, more distant, and more reddened than the previously known classical Be stars in the area. We will return to this point later on comparing the expanded sample presented here with the properties of the classical Be stars in the BeSS database and the early-type emission line stars in the catalogue of Kohoutek & Wehmeyer (1999, KW99 from now on).

In this work, we add a further 181 classical Be stars to the sample analysed in paper I. These stars have also been spectroscopically-confirmed, but with lower-resolution spectra. Our aim here is to present a homogeneous catalogue for all 248 stars, that incorporates photometry from WISE, alongside 2MASS data, and provides a sound estimate of the interstellar extinction towards each of them. The available range of data for the stars in the catalogue is presented in Section 2. The spectral typing for the new classical Be stars is described in Section 3, where we compare the results with those obtained in paper I. In Section 4, we will discuss the measurement of interstellar reddening and we will describe the procedure adopted for removing the circumstellar colour-excess from the observed $(r-i)$ colour. Finally, the discussion in Section 5 focuses on the comparison between the interstellar reddenings measured for the classical Be stars and the total integrated values for their Galactic sightlines, by Schlegel, Finkbeiner & Davis (1998, hereafter SFD98) and Rowles & Froebrich (2009, hereafter RF09), and we confront our results with the most recent 3D extinction maps of the northern Galactic plane by Sale et al. (2014).

2 THE SAMPLE

The classical Be stars in the catalogue are found in the strip of the Galactic plane, contained within $120^{\circ} \leqslant \ell \leqslant 140^{\circ}$ and $-1^{\circ} \leqslant b \leqslant +4^{\circ}$. Their spatial distribution is shown in Fig. 1, overplotted on the SFD98 extinction map of the area. As we reported in paper I, the follow-up spectroscopy targeted Hα emitters, identified in IPHAS mainly by Witham et al. (2008). The great majority of our sample falls in the magnitude range $12.5 < r < 16.5$ (noting that the IPHAS survey is calibrated in the Vega system). In terms of the optical spectroscopy we have available, the sample falls into two groups:

- 181 objects were identified in the initial follow-up optical spectroscopy, presented in Section 2 of paper I and taken no further. Observations were taken in queue mode between 2005 and 2011 at the 1.5 m Fred Laurence Whipple Observatory (FLWO)

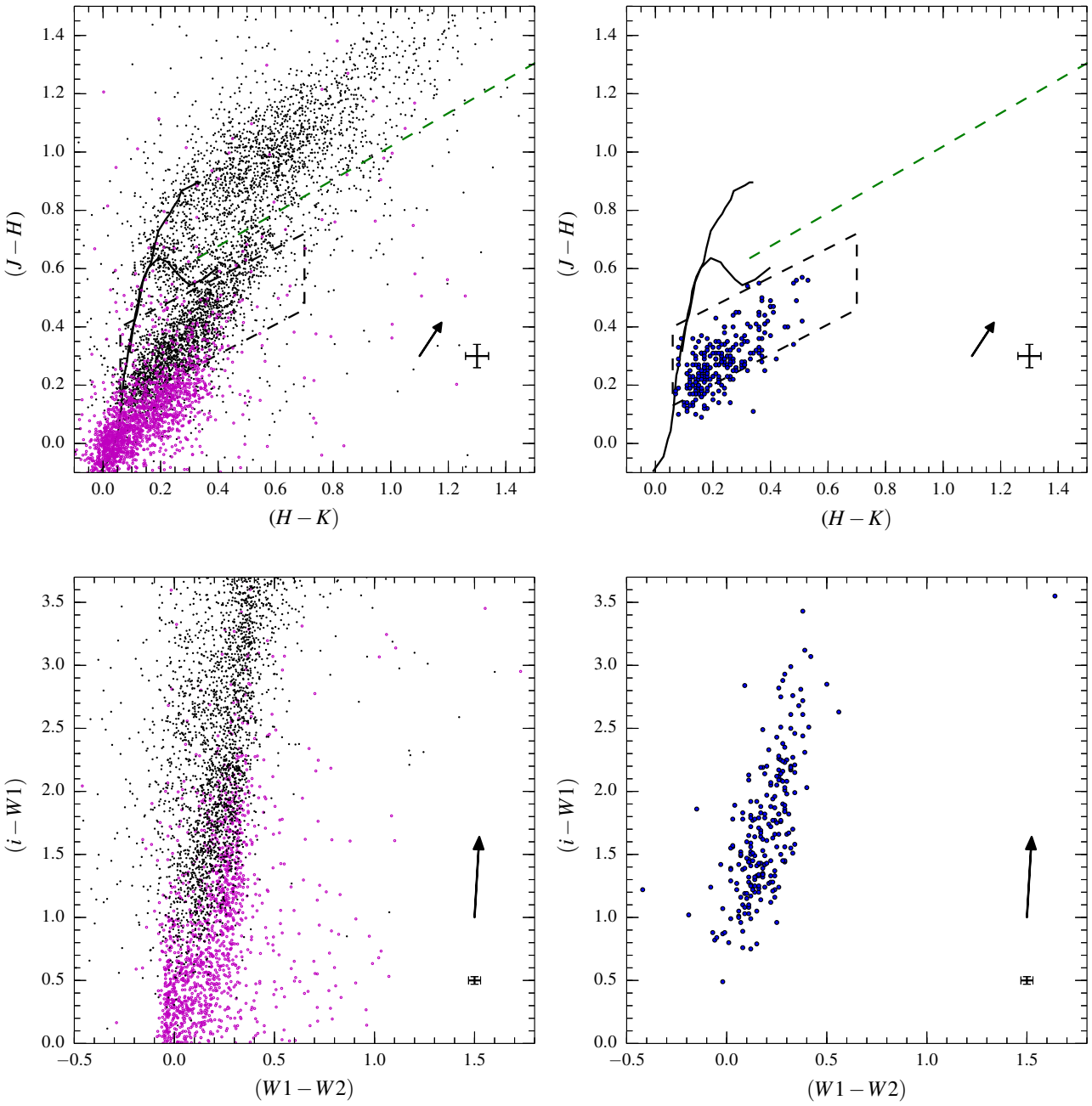

Figure 2. The top panels present the 2MASS near-IR colour-colour diagrams. The studied classical Be stars are plotted as blue circles in the right-hand panel, while on the left the Witham et al. (2008) catalogue of Hα emitters is shown in black (from which most of the classical Be stars sample is drawn) and the classical Be stars from the catalogue of Neiner et al. (2011) in lilac. The black/solid curves sketched in the top panels are the MS and giant-star loci from Rieke & Lebofsky (1985), while the green-dashed line is the classical T Tauri star locus (Meyer et al. 1997) and the black-dashed box is the generously-defined zone in which classical Be stars with $A_V = 4$ would fall (Corradi et al. 2008). The lower panels present the optical-WISE colour-colour counterparts to those shown in the top panels. The average photometric uncertainties are shown in the bottom-right corner of each plot. The black arrows are the reddening vectors for $A_V = 1$.

using the FAst Spectrograph for the Tillinghast Telescope (FAST) (Fabricant et al. 1998) and processed at the Telescope Data Centre of the Smithsonian Astrophysical Observatory. The final spectral resolution is $\Delta\lambda \approx 6$ Å and the spectral coverage is 3500-7500 Å. Since the principal aim of this initial follow-up was the characterisation of $(r - \mathrm{H}\alpha)$ excess objects identified by IPHAS at $r \lesssim 17$, the standards needed for nightly flux calibration were not obtained.

- 67 objects are the sample of confirmed classical Be stars, observed using the INT and Nordic Optical Telescope in La Palma, that were studied in depth in paper I. For 60 of them, FLWO-1.5m/FAST spectra are also available. Details regarding the selection and observation of this sub-sample are given in Sections 2 and 3 of that paper, while their spectral typing is described there in Section 4. The spectral resolution of the La Palma data is 2–3 times

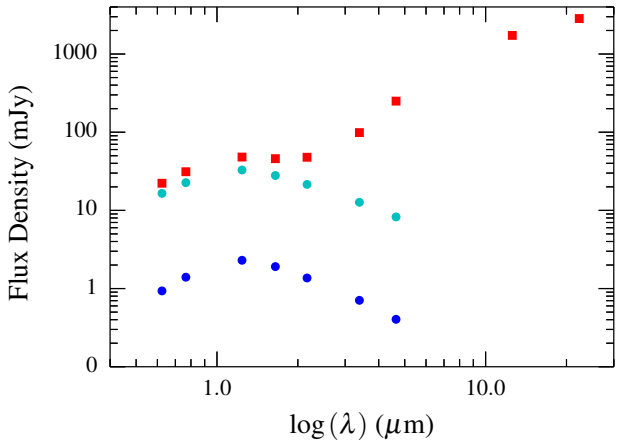

Figure 3. The 0.6 – 5 μm SEDs of three objects in the catalogue. Red squares are used for # 174 that we rule out as classical Be star, because its SED suggests the presence of warm dust. For this object we plot the WISE W3 and W4 fluxes, which were also available. The other two SEDs shown are for two typical classical Be stars in our sample, i.e. # 44, and # 184.

higher than that delivered by the FAST instrument, and sufficient flux standards were observed to permit relative spectrophotometry. These stars can now provide some checks on the inferences drawn from the larger FLWO-1.5m/FAST-only sample.

The criteria satisfied by all stars in the spectroscopic sample we present are: (i) the spectrum has a B-type spectral appearance with the low-order Balmer lines in emission – Hα-emission is necessary for identification – and no clearly visible forbidden emission lines (Porter & Rivinius 2003; Rivinius et al. 2013); (ii) the near-IR colours are consistent with those of classical Be stars; (iii) $(J-H) \leqslant 0.6$ (see e.g. Corradi et al. 2008, and top right panel of Fig. 2).

To better confirm the classical Be nature of the stars in our sample, we now complement the IPHAS and near-IR photometry from the Two-Micron All-Sky Survey (2MASS, Skrutskie et al. 2006), with $W1$ (3.4μm) and $W2$ (4.6μm) data from the Wide-field IR Survey Explorer (WISE, Wright et al. 2010). The combination of optical and near-IR colours, plotted against $(W1-W2)$ colours from WISE, can reveal the presence of a warm dust shell that would imply the object is more likely to be a young Herbig Be star. The circumstellar contribution to the near- and mid-IR spectral energy distribution (SED) of a classical Be star is very small in comparison to that seen in dust-enshrouded Herbig and other more exotic Be stars (Gehrz et al. 1974; Dachs et al. 1988; Waters et al. 1991; Lada & Adams 1992). One would expect the stars in our sample to be stretched over a relatively limited portion of the colour-colour diagrams of Fig. 2, chiefly due to the effect of interstellar reddening. That is, their locus should roughly parallel the reddening vector – which they do, in both panels of Fig. 2. The expectation regarding the SEDs of classical Be stars is that they do *not* present the double-peaked appearance or the flat/rising profile through the 1–5 μm range, that is typical of young stellar objects (YSOs).

It turns out that the added WISE photometry mainly confirms the results of the classification via a combination of visual inspection of optical spectra and 2MASS photometric criteria employed in paper I. Just one object, star # 174 (# 45 in paper I) is excluded on the basis of its $W1$ and $W2$ magnitudes. This object is more likely to be a Herbig Be star approaching the zero-age MS: its $(W1-W2)$ colour is very extreme, placing it in the top right corner of the upper-right panel of Fig 2. For comparison, we plot in Fig. 3 the SED of star # 174 together with the SEDs of two more typical classical Be stars in our catalogue. While the SEDs of the two classical Be stars do not present a marked circumstellar colour-excess out to $\sim 5\mu$m, the SED of # 174 rises strongly through the WISE bands indicating the presence of warm dust. In addition, a few objects are found to have $(W1-W2) < 0$, which does not make physical sense even for early-type stars. Although in most cases their colours are consistent with zero (to within 3 times the quoted errors), the WISE team note a tendency to overestimate the background subtraction and, as a result, underestimate the magnitudes when $W1 > 14$ and $W2 > 13.5$. This is plausibly the source of difficulty for objects # 127, 135, and 229 that show the largest negative values.

Finally, we also identify 6 objects in common with Koenig et al. (2008) (# 212, 222, 223, 225, 230, and 234 in Table 1). The authors used Spitzer near- and mid-IR photometry to classify the YSOs belonging to the star forming region W5. Their classification is determined from the slope of the SEDs in the 1.25–24 μm range, after correcting for foreground extinction via the use of 2MASS-generated extinction maps (Gutermuth et al. 2005, and references therein). Sources # 222, 230, and 234 are labelled as class III, i.e. objects that are dominated even at IR wavelengths by photospheric emission. This is consistent with the classical Be-star definition. On the other hand, # 212, 223, and 225 are labelled as class II YSOs, which means the emission from the circumstellar disc in the IR dominates over the photospheric emission, as seen in T Tauri stars or Herbig Ae/Be stars with optically thick discs. We question this classification, noting that the colours of these objects in the Spitzer colour-colour diagrams of fig. 5 and 6 in Koenig et al. (2008) overlap with objects that the authors identify as transition-disc and class III. They do not stand out in Fig. 2. Our sample also includes one star (# 217) that falls within the area surveyed by Koenig et al. (2008) that does not find a match with their sources. This object is reported to vary in the WISE source catalogue and, indeed, the listed $W1$ and $W2$ fluxes are at odds with both 2MASS and IPHAS photometric data, in being much brighter than extrapolation would suggest. Neither 2MASS nor WISE images show evidence for nearby blended sources.

In Table A1, we report the photometry for all the 248 stars in the sample. Star # 174 is included in this list, but it will be excluded from further analysis. Unless otherwise noted, the r, i, and Hα magnitudes given here take advantage of the most recent IPHAS release (DR2, Barentsen et al. 2014). We also indicate whether a star in the catalogue has a La Palma spectrum, a FLWO-1.5m/FAST spectrum, or both.

2.1 Completeness and a comparison with previous catalogues

The selection and identification of classical Be stars from IPHAS photometry, is limited mainly by the combination of interstellar reddening and the strength of Hα emission. In other words the likelihood of inclusion in the sample can be defined with reference to $(r-i)$ colour (dominantly a measure of extinction for B stars), and $(r-\mathrm{H}\alpha)$ excess (which is proportional to emission equivalent width $EW(\mathrm{H}\alpha)$). From the IPHAS colour-colour plane plotted in Fig. 4, it can be estimated that the sample is reasonably complete down to $EW(\mathrm{H}\alpha) \lesssim -15$ Å over the colour excess range, $0.5 \lesssim E(B-V) \lesssim 1.5$. Note, however, that objects with weaker line emission can be selected in the lower half of the reddening range – as long as they remain fainter than $r \sim 12$ (the saturation limit of IPHAS). Indeed the bright limit potentially cuts out some modestly reddened B0-B1 classical Be stars. In principle, classi-

Table 1. Classical Be stars with matching entries within a 5-arcsec search radius in Koenig et al. (2008). Ours and their ID number (recno) are given for each, along with IPHAS *r* and Spitzer magnitudes and YSO class according to Koenig et al. (2008).

N	recno	IPHAS2 *r* (mag)	3.6 μm (mag)	4.5 μm (mag)	5.8 μm (mag)	8.0 μm (mag)	24 μm (mag)	class	Separation (arcsec)
212	2833	13.37	9.78 ± 0.01	9.55 ± 0.01	9.25 ± 0.01	8.95 ± 0.01	7.78 ± 0.04	II	0.10
222	10258	16.17	12.83 ± 0.01	12.69 ± 0.01	12.53 ± 0.05	12.06 ± 0.12		III	0.04
223	10573	14.52	11.93 ± 0.01	11.57 ± 0.01	11.24 ± 0.01	10.76 ± 0.03	9.10 ± 0.08	II	0.70
225	12190	15.01	12.07 ± 0.01	11.81 ± 0.01	11.54 ± 0.02	11.21 ± 0.02		II	0.21
230	15241	13.88	11.80 ± 0.01	11.59 ± 0.01	11.40 ± 0.01	11.11 ± 0.03		III	0.09
234	16947	14.38	12.14 ± 0.01	11.95 ± 0.01	11.73 ± 0.01	11.51 ± 0.04		III	0.08

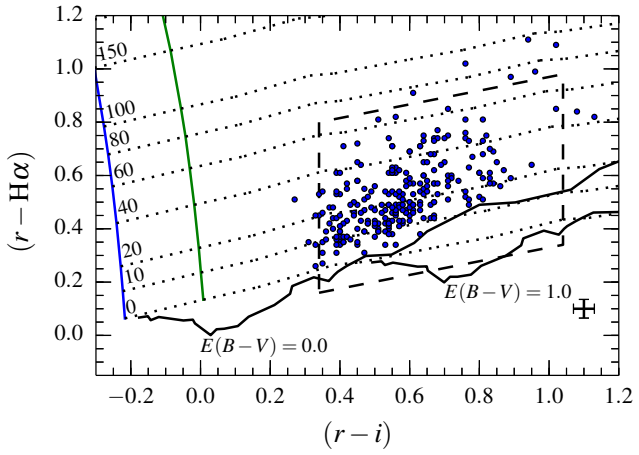

Figure 4. IPHAS colour-colour diagram of the 248 objects studied here (blue symbols). The black thin-curves are synthetic main sequence (MS) loci (see table 2 in Drew et al. 2005). The lower dashed curve is the early-A reddening curve, while the dot-dashed curves are lines of constant Hα emission (corresponding equivalent widths are indicated on the left-hand-side of the plot). The vertical curves are the curves of growth of Hα emission for the Rayleigh-Jeans case (blue, $F_\lambda \sim \lambda^{-4}$) and an A0V SED (green, $F_\lambda \sim \lambda^{-3}$). The thick black line, for an equivalent width of $EW(\mathrm{H}\alpha) = -15$ Å represents the completeness limit for $E(B-V) = 1$. On the bottom right side of the figure, the mean colour uncertainties are indicate. For reference, we also overplot the expected domain for classical Be stars with $A_V = 4$ (Corradi et al. 2008), as a black-dashed box.

cal Be stars more reddened than $E(B-V) \sim 1.5$ can be picked out if they present with correspondingly stronger Hα emission, lifting $(r-H\alpha)$ above the main locus of late-type MS stars. There are no such candidates in the present magnitude-limited sample.

Comparing our sample with previously known classical Be stars gives some insight into the photometric selection and how the bright and faint magnitude limits ($r \approx 17$) affect the outcome. In the area there are 64 known classical Be stars listed in the BeSS database, plus 148 Hα emitters in the KW99 catalogue, with spectral types and near-IR colours that match our classical Be star definition. These two databases have in common 45 objects, while the overlap with our sample is only 13 objects cross-matching within 5-arcsec (in Table 2). The matches generally have *V* magnitudes within a few tenths of the IPHAS2 *r* magnitudes, as should occur if they refer to the same object. Also these stars are all sufficiently isolated in the IPHAS images, relative to other similarly bright stars, that we can have confidence in the cross-identification.

This modest overlap mainly reflects the magnitude ranges sampled, as is evident from the distributions plotted in Fig.5. The stars in our new catalogue are on average 2-3 magnitudes fainter

Table 2. Classical Be stars with matching entries within 5-arcsec in the KW99 and BeSS catalogues. Their visual magnitudes and spectral types (from KW99) and angular separation are supplied along with the ID name and coordinates. The IPHAS2 *r* magnitudes, calibrated in the Vega system, are brought forward from the full photometry list, Table A1.

N	(KW99)	BeSS	*V* (mag)	SpT	IPHAS2 *r* (mag)	Separation (arcsec)
8	3-27		15.1		14.85	4.0
37	5- 3		14.6	A	12.64	2.9
73	7-25		12.4	B	12.46	1.0
74	7-31	SAN 28	13.4	B	13.76	0.3
76		BG 82			13.37	0.1
115	9- 7		13.9		13.40	1.8
124	9-29		12.9		12.58	2.3
144	9-55				12.87	3.2
174	12-38		12.5		12.88	4.2
186	12-58		13.6		13.26	0.2
205	13-31				13.43	0.5
208	13-36		12.5		12.91	0.5
244	14-40		15.1		14.46	0.9

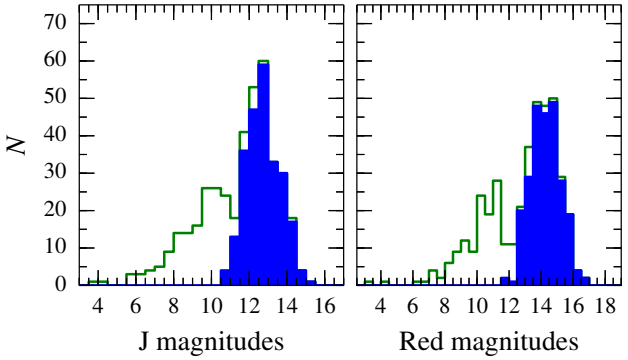

Figure 5. 2MASS *J* and red magnitudes distributions, for the 248 classical Be stars in the sample (solid blue) and for the previously known classical Be stars in the area (step histogram). Not all the previously known classical Be stars have 2MASS photometry so that only 152 are plotted in the left figure. Because fewer of the previously known classical Be stars in the area do not possess IPHAS *r* photometry either, we used USNO B1.0 photometry (Monet et al. 2003) as a close proxy.

than in either the BeSS database or KW99. We notice that the merged magnitude distributions seem to peak at 12-13 mags in J and 14-15 mags in the red, but present a deficit of stars at respectively $J \approx 11$ and $R \approx 12$. This feature may very well be due to the combined incompleteness of KW99 and Witham et al. (2008) lists,

in particular, at the intersection of their faint and bright limits. Furthermore, the median magnitudes of classical Be stars in the BeSS catalogue in this same region are also relatively bright at $R \sim 10$ and $J \sim 9$. It can be inferred that, if the magnitude distributions are smooth, in reality, there remains a deficit of 30-40 classical Be stars at $r \sim 12$ awaiting discovery.

3 SPECTRAL TYPING OF THE FLWO-1.5m/FAST SAMPLE

Compared to the classification of the La Palma spectra reported in paper I, classification based only on FLWO-1.5m/FAST spectra is more challenging, due to the generally lower S/N ratio – with a median of S/N = 28, at λ4500 Å – and lower spectral resolution. However, for the purpose of determining interstellar reddenings from IPHAS $(r-i)$ colours, even a coarser spectral type assignment, as opposed to the precision of 1-2 sub-types reached in paper I, is still acceptable, due to the weak dependence of intrinsic $(r-i)$ colours on spectral type among B-type stars (see also Section 4).

Here, we will estimate spectral types relying on the most easily detected blue spectral features – the He I (λ4471 Å) and Mg II (λ4481 Å) lines – alongside the higher Balmer series.

We stressed in paper I the value of measuring the ratio of equivalent widths, $\log(W_{\lambda4471}/W_{\lambda4481})$, as it is well established as a guide to effective temperature. We also showed before that the reliability of the measure is strongly dependent on the S/N ratio measured in the proximity of the He I and Mg II transitions, finding in particular that for spectra with S/N lower than ~ 25 there is a marked increase in the spectral typing error, and that at $S/N \sim 10$ almost no constraint is possible. This evaluation was based on measuring line ratios from model atmospheres (Munari et al. 2005) many times, to which controlled amounts of random noise had been added. For $S/N \geqslant 25$ the distribution of measured line ratios from model atmospheres was found to be sufficiently narrow to allow a spectral-type determination within 1-2 subtypes.

Our approach to typing here has to be effective on less optimal data. Where we can, we assign a trial spectral type from measurement of the $\log(W_{\lambda4471}/W_{\lambda4481})$ ratio, and otherwise appraise types by means of comparisons with model spectra (Munari et al. 2005). The spectral classification of the classical Be stars arising from both FLWO-1.5m/FAST spectra and the La Palma data presented in paper I have been compared, to check for overall consistency of outcome: this confirms that typing to within 1-2 subtypes starts failing at $S/N \sim 25$ (we return to this at the end of this section). Hence we have split the FLWO-1.5m/FAST sample into two, according to S/N ratio: (i) for spectra with $S/N \geqslant 25$, we use $\log(W_{\lambda4471}/W_{\lambda4481})$, as an effective temperature proxy, and then check via comparison with model atmospheres; (ii) for the spectra with $S/N < 25$ and some better-exposed cases where method (i) gives uncertain solutions, we are restricted to assessing the best spectral type via a simple χ^2 minimisation, using resolution-degraded Munari et al. (2005) model atmospheres. To facilitate (ii), both the observed spectrum and the models are normalised to unity over the spectral range $\lambda\lambda\,3800-5000$ Å. In Fig. 6, three examples with decreasing S/N ratio at λ4500Å are given. The agreement is convincing for the spectra shown in the top two panels while the classification of the least well-exposed example is clearly much more uncertain.

We have found that spectral types assigned with method (i) rarely needed a sub-type shift of more than a 1-2 sub-types, in order to better satisfy a visual comparison with model spectra. Where a star has been observed at higher resolution from La Palma, we continue to use the La Palma spectral typing for the purpose of estimating reddenings in Section 4. We also note that 3 stars (# 73, 74, 76) of the 181 stars with FLWO-1.5m/FAST spectra were already classified by Mathew & Subramaniam (2011) as B2V, B5-7V, and B5V, to be compared with our B2, B4, and B3 spectral types (these three stars are also found in KW99 and in the BeSS catalogue, e.g. cf Table 2).

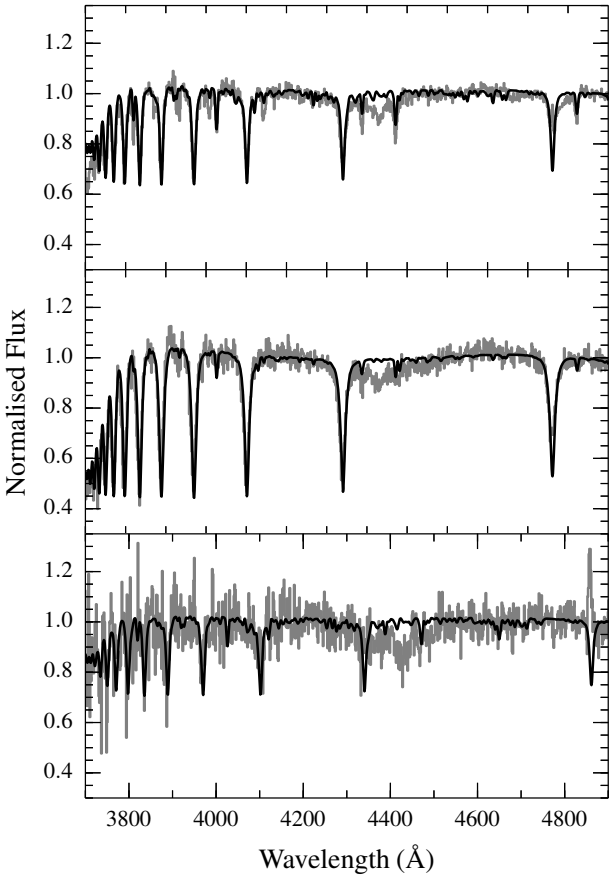

Figure 6. Three example of spectra observed with FLWO-1.5m/FAST are shown. From top to bottom: # 121 is a B3 star with S/N = 62; # 183 is a B7 star, with S/N = 45; # 115 is an Early-B type star with S/N = 20. The observed spectra are plotted in grey, while the appropriate model atmospheres from Munari et al. (2005) are in black.

On the other hand, for the spectra with $S/N < 25$ that were classified with method (ii), the grid of Munari et al. (2005) models that we used is limited to $\log g = 4$, rotational velocity of 250 km/s (typically observed in Be stars, Chauville et al. 2001), and $T_{\rm eff} = 9000$–30000 K, which we map onto spectral types using the Kenyon & Hartmann (1995) scale. In the minimisation procedure, we masked out the Hβ, and Hγ spectral regions that can be more strongly affected by emission/infilling, along with the spectral region between λλ 4400–4500 Å that includes the diffuse interstellar band at λ 4428 Å (often strong in our spectra, whilst absent from the model atmospheres). Including the Balmer jump helps the spectral-type determination, since the jump itself carries a $T_{\rm eff}$ dependence. Since the final output of the χ^2 minimisation does not allow a typing better than 3-subtypes on average, we classified the stars put through method (ii) as one of Early-B (B0 to B3), Mid-B (B4 to B6), or Late-B (B7 to A0), according to the range in which the

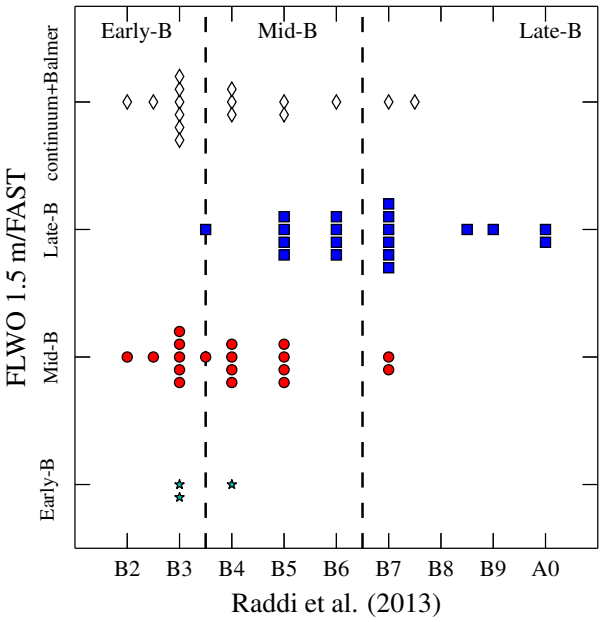

Figure 7. Comparison between spectral types determined from La Palma spectra and from FLWO-1.5m/FAST observations, where S/N < 25 (using method ii). The latter are grouped as explained in the text.

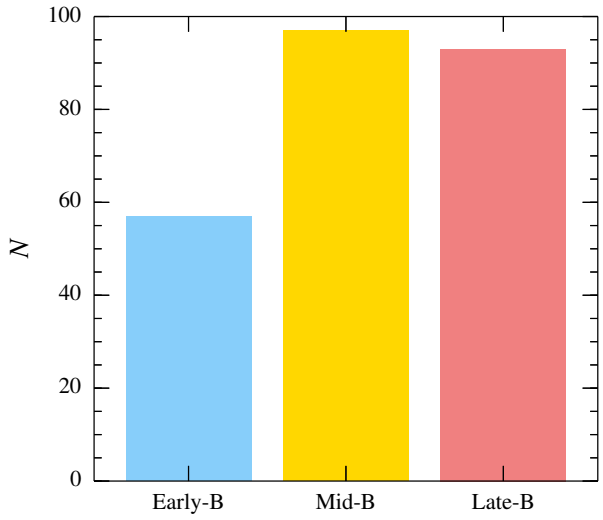

Figure 8. Grouping of spectral types of the 247 classical Be stars in the catalogue. Early-B: B1–B3, Mid-B: B4–B6, Late-B: B7–A0.

measured minimum χ^2 falls. In cases where the FLWO 1.5m/FAST spectra are relatively underexposed (S/N $\sim$ 10), they are classified even more loosely as "continuum+Balmer line emission"

The spectral types assigned to the FLWO-1.5m/FAST spectra and the S/N ratio at λ4500 Å are given in Table B1 along with the spectral types and S/N ratio measured for the La Palma spectra in paper I.

The comparison between the spectral types that are determined with method (ii) and more precisely from paper I La Palma spectra is shown in Fig. 7. This offers a useful insight into the dataset. The FLWO-1.5m/FAST classifications are broadly consistent, with the expected large scatter and perhaps a slight tendency to shift to later type. Interestingly, the spectra classified as "continuum+Balmer line emission" are revealed by the superior La Palma data to be overwhelmingly early and mid B sub-type – a finding that may fit with their being more distant, more highly-reddened (tougher to observe) objects.

To conclude, we display the spectral type distribution of the 247 classical Be stars in Fig. 8, arranging them as Early-B, Mid-B, and Late-B types. The distribution is fairly even between types, with the Early-B group being less populous than the other two, accounting for around a quarter of the sample. This modest favouring of later types stands in interesting contrast with the distribution by type present in the BeSS catalogue in which around half of the objects are B3 or earlier (Neiner et al. 2011). This may originate in small part from the spectral-typing bias we find affecting the FLWO-1.5m/FAST spectra (Fig. 7). However it is also true that previous studies on Be stars have focused on brighter, magnitude-limited samples, compared to our search that reaches to fainter magnitudes and takes the surveyed volume more closely to the limits of the Galactic disc (see Section 5). Furthermore, it is worth noting that the impact of interstellar extinction on our method of selection should be to favour earlier-type classical Be stars with stronger Hα emission. The fact that now the earlier-type classical Be stars are a minority group hints that few B0-B3 stars remain to be discovered at fainter magnitudes.

4 INTERSTELLAR REDDENING

In paper I, we adopted a spectroscopic method for measuring the $(B-V)$ colour excesses of 67 classical Be stars, from well flux-calibrated spectra. As part of the confirmation that these stars are classical Be stars, we also determined the $(B-V)$ colour excesses indirectly by using IPHAS $r, i,$ Hα photometry. The expectation that colour excesses inferred from IPHAS photometry were larger than the direct blue/visual SED-fitting was confirmed – indicating the SED-reddening presence of circumstellar emission, usually interpreted as evidence for discs around these stars. Paper I adapted existing methodologies for the correction of the measurements for the effects of the characteristic superposed disc emission. Here we compute colour excesses for the entire FLWO-1.5m/FAST sample using the photometric approach, because the spectra do not offer a reliable flux calibration.

The excess in the $(r-i)$ colour can be written as:

$$E(r-i) = (r-i) - (r-i)_\circ \qquad (1)$$

The intrinsic-colour scale we adopt is the same we used in paper I. Because the red-optical SED of B-type stars tends towards the Rayleigh-Jeans limit of the Planck function, the intrinsic colour $(r-i)_\circ$ is not very sensitive to effective temperature: across the complete B0 to A0 range, it changes from -0.17 to 0.0. This implies that even if spectral types determined from FLWO-1.5m/FAST spectra are more uncertain than those derived from better-resolved La Palma spectra, the intrinsic colour we assign to any one star will typically carry uncertainty of ± 0.05.

The measured colour excess, $E(r-i)$, of Eq. 1, includes a circumstellar contribution, $E^{cs}(r-i)$, along with the dominant interstellar component, $E^{is}(r-i)$:

$$E(r-i) = E^{is}(r-i) + E^{cs}(r-i), \qquad (2)$$

as is true also of the $(B-V)$ colour excess (e.g. Dachs et al. 1988;

Table 3. Circumstellar colour excess $E^{is}(r-i)$, estimated for a given spectral type and disc contribution to the total flux.

SpT	$T_e(K)$	$f_D = 0.05$	$f_D = 0.10$	$f_D = 0.20$	$f_D = 0.30$
B1	18000	0.055	0.106	0.194	0.269
B3	13200	0.063	0.119	0.216	0.297
B5	9300	0.071	0.134	0.240	0.328
B7	7800	0.082	0.153	0.272	0.367
A0	5700	0.112	0.205	0.352	0.464

Kaiser 1989). The disc emission at red wavelengths produces a contribution to the colour excess that is larger than the disc emission in the $(B-V)$ colour we corrected for in paper I. In order to estimate the $E^{cs}(r-i)$, we use the grid of recombination continua that was modelled in paper I, to represent the disc emission. The grid of models has been generated for 10 different spectral types, with the electron temperatures in the circumstellar disc scaling to the stellar effective temperature according to $T_e = 0.6 \times T_{\rm eff}$ (as is typically observed in both hot-star winds and classical Be star discs, Drew 1989; Carciofi & Bjorkman 2006), and for finely spaced (0.01 dex) disc fractions f_D. The latter quantity specifies the ratio between the disc flux and the total flux emitted by the star and disc together at $\lambda\,5500$ Å. The circumstellar continuum excess, in $(r-i)$, is defined as:

$$E^{cs}(r-i) = (r-i)_{\rm star+disc} - (r-i)_{\rm star}. \quad (3)$$

The theoretical values for different combinations of T_e and f_D are determined by convolving the IPHAS filters' profiles with both the star+disc and star-only models. To model the stellar photospheres we chose the most appropriate models from the Munari et al. (2005) library. A sample of theoretical estimates is given in Table 3 as a function of the spectral type, or $T_{\rm eff}$, and f_D.

As in paper I, we estimate the appropriate circumstellar colour excesses for each star by linking the disc fraction to the $EW(\rm H\alpha)$, by means of the empirical equation:

$$f_D = 0.1 \times \frac{EW(\rm H\alpha)}{-30\,\text{Å}}, \quad (4)$$

first proposed by Dachs et al. (1988). The scatter associated with Eq. 4 is about ~ 0.02 dex. To maintain contemporaneity between the measures of $E(r-i)$ and f_D, we estimated $EW(\rm H\alpha)$ by interpolating the IPHAS colours between the theoretical curves of growth that were plotted in Fig. 4 and computed in Drew et al. (2005). In Table B1, we give all the derived and measured quantities used in obtaining the estimates of $E^{cs}(r-i)$ and $E^{is}(r-i)$ via Eq. 1–4. Since interstellar reddenings are generally expressed as the colour excess in the $(B-V)$ colour, we compute it using the following transformation:

$$E^{is}(B-V) = \frac{E^{is}(r-i)}{0.65}, \quad (5)$$

where 0.65 is the monochromatic conversion-factor[2], computed from the Fitzpatrick (1999) $R_V = 3.1$ reddening law. The errors on $E^{is}(B-V)$ are typically in the range of 0.05–0.1 mag. They combine the IPHAS photometric uncertainty, an uncertainty on spectral type, the astrophysical spread of intrinsic colours for MS stars (Houk et al. 1997), and the uncertainty arising from the estimate of disc fraction.

[2] The conversion factor is 5 per cent smaller than the band-averaged value of 0.69 that we used in paper I.

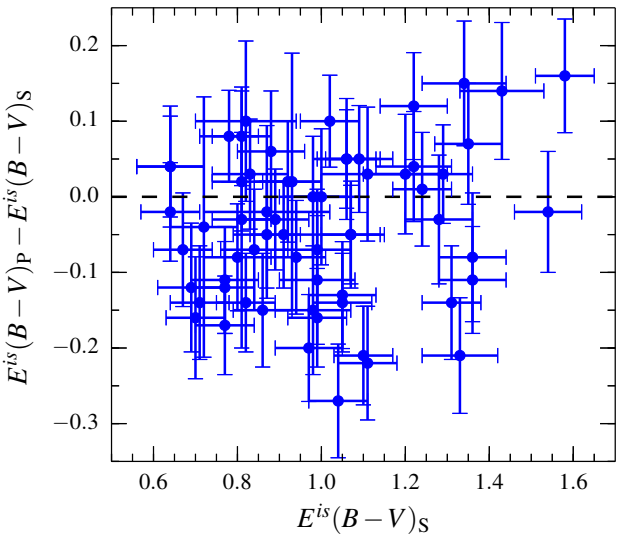

Figure 9. The difference between the two estimates of interstellar reddenings, for the 63 classical Be stars with La Palma spectra, are plotted against the $E^{is}(B-V)_{\rm S}$ determined via SED fitting to the blue spectral region (paper I). The equality line is also shown. The mean difference is found to be $\sim -0.04 \pm 0.01$.

For 63 of the 67 classical Be stars that were observed in La Palma, the interstellar reddenings derived in the first place via the SED fitting procedure of paper I are compared to the photometric procedure described here, in Fig. 9. From the comparison, we notice a systematic negative difference: the mean offset being $\Delta E^{is}(B-V) = -0.04 \pm 0.01$, with a sample standard deviation of 0.1 mag. This is just significant at the 3σ level, and it may connect to the impression noted in Section 2 that the spectral type estimates based on FLWO-1.5m/FAST data are inclined to be later than those based on La Palma spectra. Nevertheless the bias is not large and we will recall it in Section 5, when appropriate. The level of scatter apparent is a little high relative to the individual errors on $E(B-V)$ and may in part be due to the application of a single reddening law.

The distribution of derived $E^{is}(B-V)$ is shown in Fig. 10. The overall mean colour excess is 0.86 mag, with a sample dispersion of 0.23 mag. We first note that the median $(B-V)$ colour excess, measured for the group of Early-B stars, is found at 0.98 mags that is larger than the median values of $E^{is}(B-V) = 0.83,\ 0.78$ obtained for the Mid-B and Late-B groups. This difference is not surprising, as the intrinsically brighter group of stars can be detected behind a larger column of dust. We also note that the stars observed in La Palma are on average more reddened and therefore fainter (median $E^{is}(B-V) = 1$, and $r = 14.7$) than the FLWO-1.5m/FAST objects, for which the distribution medians are $E^{is}(B-V) = 0.81$ and $r = 14$. This difference arising from the larger aperture offered by the INT with respect to the FLWO-1.5m. The median contribution to the $(r-i)$ colour excess due to the circumstellar disc is 0.11 mag, reflecting a median disc fraction, f_D, of 0.07.

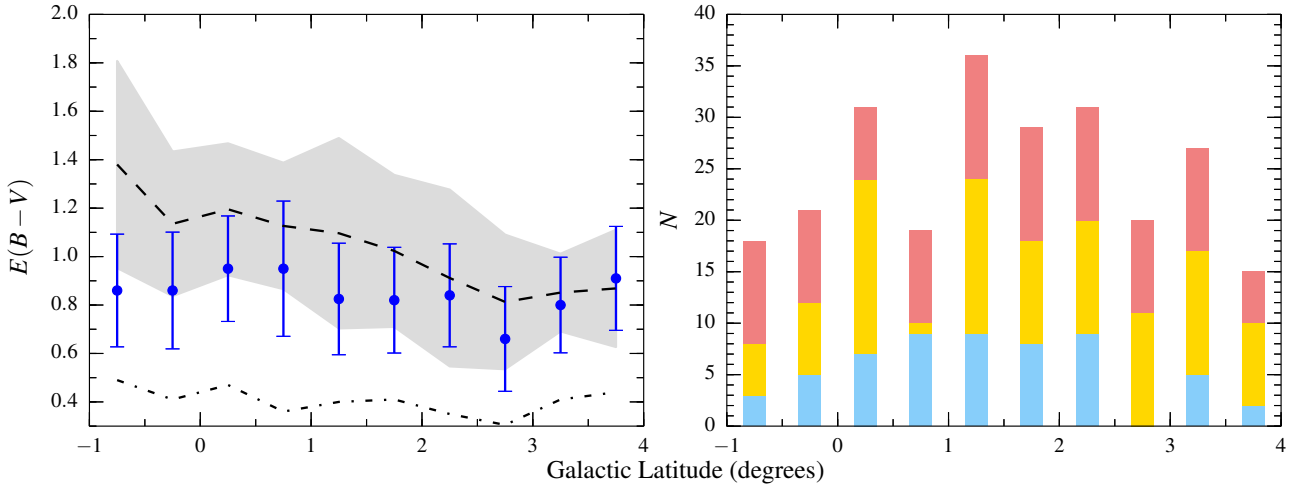

Figure 11. Left panel: mean interstellar reddenings derived from the 247 classical Be stars in the catalogue on binning up into 0.5 deg strips parallel to the Galactic plane (marginalising over longitude). The error bars represent the 1-σ dispersion around the mean values. The upper dashed-curve and the shaded area trace the mean SFD98 values in each strip and the relative 1-σ dispersion, while the lower dot-dashed curve follows the mean RF09 values in each strip. Right panel: histogram bars representing the number of classical Be stars in each latitude bin, colour coded accordingly to the spectral classification (light blue: Early-B; gold: Mid-B; Late-B: pink).

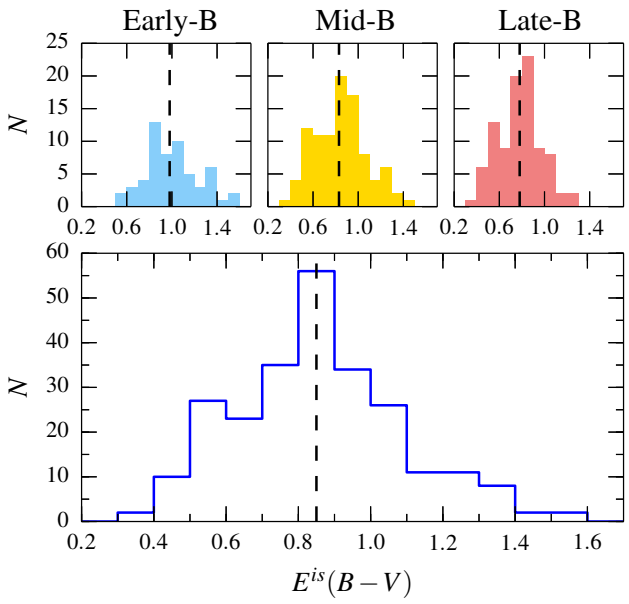

Figure 10. Histogram distribution of the photometric colour excess. In the top panels, objects are sorted by spectral-type groups, while the bottom panel shows the combined distribution. The overall mean is found at $E^{is}(B-V) = 0.86 \pm 0.23$, and the dashed lines mark the median of each distribution.

5 INFERENCES ON THE SPATIAL DISTRIBUTION OF THE CLASSICAL BE STARS SAMPLE FROM INTERSTELLAR EXTINCTION

Armed with approximate spectral types, we have derived interstellar colour excesses across the sample to a median precision of $\Delta E(B-V) = 0.08$, after making the necessary correction for circumstellar emission. This typical uncertainty is in the region of 10 per cent of the typical reddening towards these stars. It allows more than enough precision to make a broad comparison with existing measures of integrated extinction in the area in order to gain a first impression of how the population of classical Be stars is distributed. To achieve this, we turn to comparisons with three comprehensive studies of the pattern of Galactic-Plane extinction – namely, SFD98, RF09, and Sale et al. (2014).

To begin with, we recall some constraints from studies of open clusters. The lowest classical Be star reddenings obtained here are compatible with less obscured parts of the Perseus Arm, such as the sightline to the open cluster NGC 637 with $E(B-V) \sim 0.6$ (Maciejewski & Niedzielski 2007). The average colour excesses resemble those measured for more prominent clusters in the Perseus Arm, such as $E(B-V) \simeq 0.8$ mag for both IC 1805 (Massey, Johnson & Degioia-Eastwood 1995) and NGC 663 (Pandey et al. 2005). If we consider all the open clusters in the Dias et al. (2002) catalogue seen in this part of the Galactic Plane, we find that clusters in the range of distances that is regarded as typical of the Perseus Arm (i.e. 2–3 kpc Russeil, Adami & Georgelin 2007; Vallée 2014) are also reddened on average by 0.8 mags, although the full range runs from 0.3 up to 1.2. The high-end extinctions tend to be associated with IR-identified clusters. Clusters listed by Dias et al. (2002) at greater distances have colour excesses only a little larger, spanning 0.5 up to 1.3 mag. In view of this it is reasonable to anticipate that the great majority of classical Be stars identified here are at least as distant as the Perseus Arm, and some may be appreciably more distant still.

The left panel of Fig. 11 illustrates the binned distribution of reddenings per Galactic latitude range. The stars have been grouped into strips 0.5 deg wide in Galactic latitude and the median and standard deviation of the reddenings obtained within each is shown. We also plot the median values within these same strips of the total Galactic reddening obtained from SFD98 and that inferred by RF09 from median 2MASS near-IR colour excesses, along the same sets of sightlines. The SFD98 results have been adjusted using the finding of Schlafly et al. (2010) that they should be scaled down by multiplying by a factor of 0.86. In the left panel of Fig. 11 it can be seen that there is only a ~ 0.25 mag difference between the maxi-

mum classical Be star median reddening, obtained between $b = 0°$–$0.5°$, and the minimum measured in the $b = 2.5°$–$3°$ strip. It was noted above that the overall sample mean is $E^{is}(B-V) = 0.86$. The variation is within the 1-σ dispersion present in each latitude strip, indicating no strong overall trend.

It is striking, however, that the colour excesses obtained from RF09 are systematically ∼0.5 mag lower than the ones we measure for the classical Be stars. Even at the level of comparison between the individual objects in our catalogue and the RF09 data, there are only 3 for which the latter supplies a higher reddening. The discrepancy calculated on an object-by-object basis is 0.45 ± 0.01 mag with a dispersion of 0.2 mag. In contrast, the distribution of corrected SFD98 colour excesses overlaps or exceeds the general run of our classical Be-star measures. The latter result is expected for the reason that the SFD98 maps measure the asymptotic reddening along a given sightline – the maximum colour excess expected for a star behind the Galactic dust column.

Given that $E(B-V)$ to the least obscured Perseus Arm open clusters is only infrequently as low as 0.4 mag (Dias et al. 2002), it would seem that the extinction measured with the method of RF09 is limited to sampling the column of dust between the Sun and the Perseus Arm – a half or less of the likely total Galactic column. This is in part attributable to the reliance on median near-IR extinction, and may also be a consequence of the relatively bright magnitude limits of the 2MASS survey. Unfortunately the UKIDSS surveys do not reach to this part of the Galactic plane, so it cannot be established whether the RF09 method would be sensitive to more of the column if it were applied to deeper near-IR data. The main point for now is that, despite its excellent angular resolution (2–3 arcmin), the map due to RF09 does not provide a useful comparison with our catalogue of classical Be stars.

In the right panel of Fig. 11 we plot the number distribution of classical Be stars per latitude bin, distinguishing the stars belonging to different spectral type groups. First, we notice that the stars in the catalogue are more concentrated between $b = 0°$–$3°$. Each bin includes a range of spectral types that in turn will be characterised by different extinction and distance ranges (given the common magnitude bounds used in selection, see figure 10). The overall latitude distribution crudely follows a broad Gaussian peaking near $b \simeq +1.5°$, such that there is a difference of 21 stars between the most and the least populous bins. In detail, smaller number counts are observed between $b = 0.5°$–$1°$ and between $b = 1.5°$–$2°$, due to the masking effect of the larger dust columns located near W4/W5 and Cas OB 7. The Early-B type classical Be stars seem to favour the $b = 0°$–$2.5°$ range, as one would expect for an intrinsically-brighter population able to trace the warp: Freudenreich et al 2004 showed this to lie in the $1 \lesssim b \lesssim 2$ latitude range at these longitudes (in HI and dust emission). The less-luminous later spectral types, at shorter distances, show a flatter distribution.

To permit a more detailed comparison between our measured reddenings and the corrected SFD98 values, we plot the difference between them against the SFD98 values on a star-by-star basis in the upper-left panel of Fig. 12. The outcome is not qualitatively different from the results for the smaller sample presented by paper I, although there are now more stars that are observed with reddenings significantly exceeding $[E(B-V)_{\rm SFD98} \times 0.86]$. Paper I found two stars (#i̇64 and 167 here) located well above the equality line – here, these are joined by 10 more stars (i.e. # 161, 162, 166, 182, 184, 221, 225, and 232). These stars are the most extreme with $E^{is}(B-V) - E(B-V)_{\rm SFD98} \times 0.86 > +0.3$ mag in the upper-right histogram in Fig. 12. The most likely origin of this problem is the coarser angular resolution of the dust-temperature data (∼ 1 deg) used by SFD98 to infer the dust column from far-infrared emissivity data (∼ 6 arcmin angular resolution): in the vicinity of dust warmed by strong H II region emission in the Galactic Plane, this results in underestimation of the dust column (see Schlafly et al. 2010, and Sale et al. (2014)). If we count the number of stars with reddenings that are the same or larger than the SFD98 measure, less our typical 0.1 mag uncertainty, ∼ 37 per cent (91 stars) seem to be lying at or beyond the limits of the dust disc. We measure the median of the distribution of differences to be −0.2 mag, with a standard deviation of 0.35 mags.

We now turn to the IPHAS-based extinction map of Sale et al (2014), based on *r*, *i* and Hα data on stars of spectral type earlier than K, to see if this particular limitation of SFD98 at low galactic latitudes can be overcome. In the lower-left panel of Fig. 12, the measured reddening of each star is plotted against the reddening obtained at the 90th percentile of the distance distribution derived from the nearest-neighbour extinction-distance relationships of Sale et al. (2014, see fig. 3). The result is tidier in that the lowest estimated total colour excesses have disappeared and fewer classical Be star reddenings lie far above the equality line. The angular resolution of this map in our sky area is mostly 10 or 15 arcmin, rising to 30 arcmin in the vicinity of the dark clouds, W3 and W5 (where there are not so many selected stars).

The fractal nature of the ISM imposes a differential extinction (cf. fig. 6 in Sale et al. 2014) of up to 25 per cent in the most distant bins reached by the map (expressed as a standard deviation, and shown as the shaded area in the bottom left panel of Fig. 12). From inspection, we can identify 166 objects (i.e. 67 per cent of the sample) with reddenings that fall within the shaded area, that may be regarded as consistent with the reddenings at the 90th percentile of the distance in the extinction-distance relationships of Sale et al. (2014). This sets a generous upper limit on the fraction of the classical Be stars sample likely to lie beyond most of the dust column – to be compared with 37 per cent, deduced from the SFD98 comparison. We also notice that the binned distribution of differences between the reddenings we measure and the colour excess derived from the 3D extinction map peaks at −0.14 mag (lower-right panel in Fig. 12) and its standard deviation is just 0.23 mags. We recall that our photometric method is inclined toward slight under- rather than over-estimation of classical Be-star interstellar colour excess (see Fig. 9).

However, there is a modest systematic offset between the maximum extinction estimates of SFD98 and Sale et al. (2014). For the sightlines relevant here, the median difference between the two measures is 7 percent, in the sense that the scaled SFD98 results are 1.07 times the Sale et al. (2014) values. The most obvious expression of this difference in Fig. 12 is the longer tail of objects toward higher colour excess in the upper left panel presenting the SFD98 comparison that is absent from the Sale et al. (2014) comparison. If we attempt a simple correction for this offset by multiplying the Sale et al. (2014) maximum reddenings by 1.07, before considering again how many classical Be stars have reddenings compatible with the Galactic maximum, we find the fraction of the classical Be stars sample that may be located beyond the Galactic disc dust column drops from 67 per cent to 58 per cent.

Of the three estimates (37, 58, and 67 per cent) of the fraction of the sample of classical Be stars lying behind most or all the dust column, we favour the first two. In rough terms there is a case to argue that about half of the sample fits this description.

The seeming downward trend in the data in the left panels of Fig. 12 has its origins in the magnitude limits imposed on the present sample of classical Be stars. It can be seen that at small

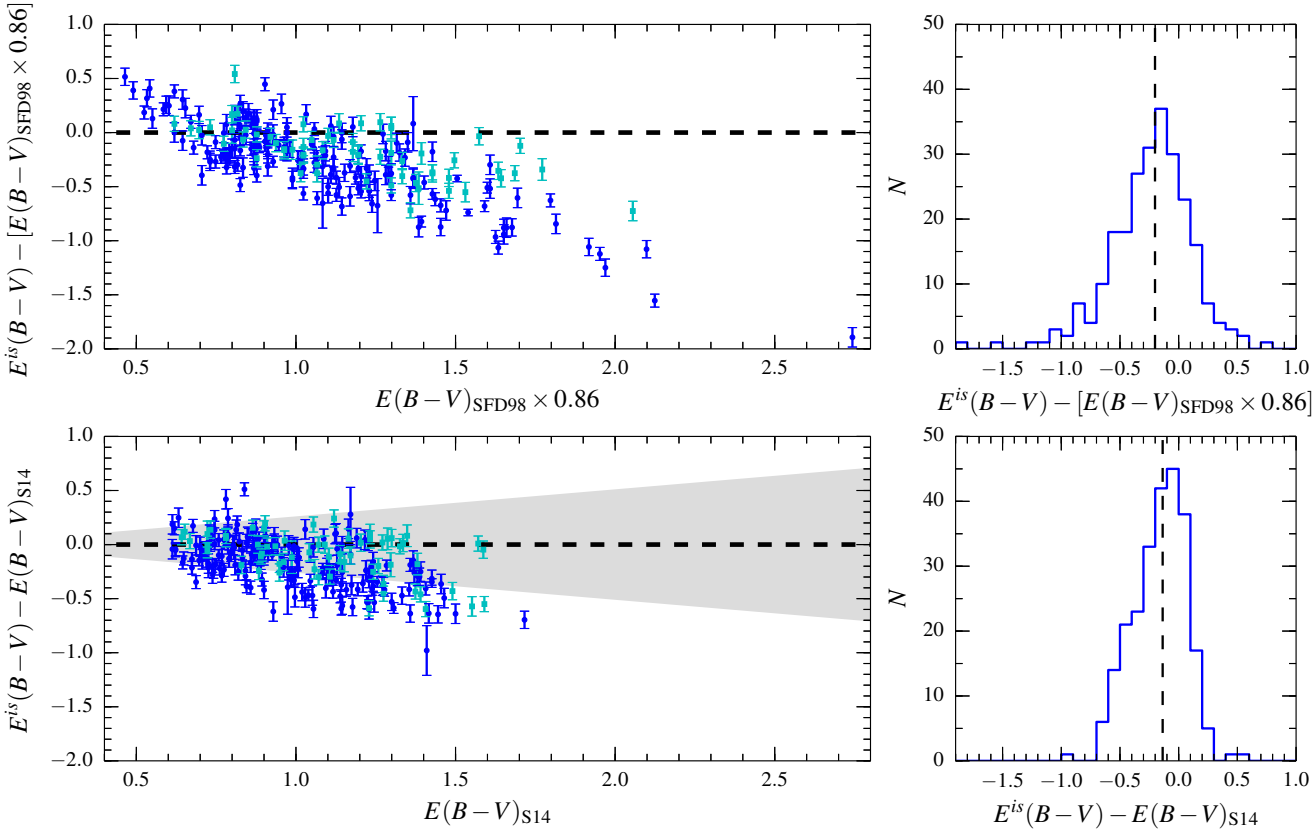

Figure 12. Upper panels: on the left, comparison between the colour excesses we measure for the classical Be stars and the values from SFD98 for the same sightlines (after applying the Schlafly et al. (2010) correction). Squares with error bars are used for the stars in paper I, while circles are plotted for the new classical Be stars presented here. The dashed line represents the equality line. On the right, is an histogram-plot displaying the collapsed difference between SFD98 and the colour excesses we measure for the classical Be stars. The dashed vertical line marks the median of the distribution at −0.2 mag. Lower panel: on the left, the same comparison with respect to the colour excess measured at the 90th percentile of the distance distribution from the 3D extinction-distance map of Sale et al. (2014). The shaded area roughly traces the scatter caused by differential extinction (cf. fig. 2 and 6 in Sale et al. 2014). On the right, the difference between the x- and y-axis is collapsed into histogram bars, with the median of the distribution at −0.14 mag as traced by the vertical dashed line.

asymptotic $E(B-V)$ the observed points cluster more tightly to the equality line than at larger asymptotic $E(B-V)$: only classical Be stars brighter than $r \sim 13^{\rm th}$ *could* be less reddened. In contrast, along the most reddened sightlines, nearer classical Be stars are picked up that present colour excesses falling progressively further below the estimate of the asymptotic limit. This is the faint magnitude limit, at $\sim 16^{\rm th}$ magnitude, expressing itself. But in both distributions, it is noteworthy that up to a $(B-V)$ colour excess of 1.4 mags, there are classical Be stars with reddenings clearly compatible with these measures of maximum reddening. We deduce from this that, along sightlines where the total Galactic colour excess is less than 1.4 mags, the classical Be stars sample is either weakly or not at all extinction-limited.

In principle, we can use the Sale et al. (2014) 3D extinction-distance relations to provide a guide to where the dust layer runs out. The reader is referred to the data available on the IPHAS survey website (www.iphas.org) to investigate any sightline of interest across this region. Nevertheless, it is not recommended to use these data to estimate distances to individual classical Be stars – the uncertainties presently involved are too large to make this worthwhile. Instead, a very simple example of spectroscopic parallax illustrates the point clearly that typical distances to them will be large, reaching beyond the Perseus Arm at 2–3 kpc: specifically, a Mid-B star ($M_r < -0.5$, paper I) of median brightness in the sample ($r \simeq 14.5$), experiencing a median extinction of $A_r \sim 2.2$, cannot lie at a shorter distance than 3.6 kpc. The faintest most reddened stars of the sample will lie at distances exceeding 6 kpc. If there is the coherent structure at these longer distances, such as the Outer Arm, then it is possible that a significant portion of the newly-identified classical Be stars, lying behind all or most of the Galactic dust column, are associated with it.

A similar conclusion was reached in paper I based on the smaller sample benefitting from higher quality spectroscopy. Indeed there it was argued that 10–15 stars in the smaller sample of 66 objects may even lie outside the Galactocentric radius of 13 kpc (or heliocentric distances larger than 7 kpc), where the Galactic stellar density gradient is expected to be steepening (Ruphy et al. 1996; Sale et al. 2010). Without question, this catalogue of classical Be stars adds many candidates to the handful of O stars proposed by other authors as belonging to the Outer Arm (e.g. Negueruela & Marco 2003).

6 SUMMARY AND CONCLUDING REMARKS

We have presented an expanded catalogue of 247 classical Be stars, drawn from a $5 \times 20\,{\rm deg}^2$ section of the Galactic Plane including the Perseus Arm and its much-studied W3–5 star-forming clouds.

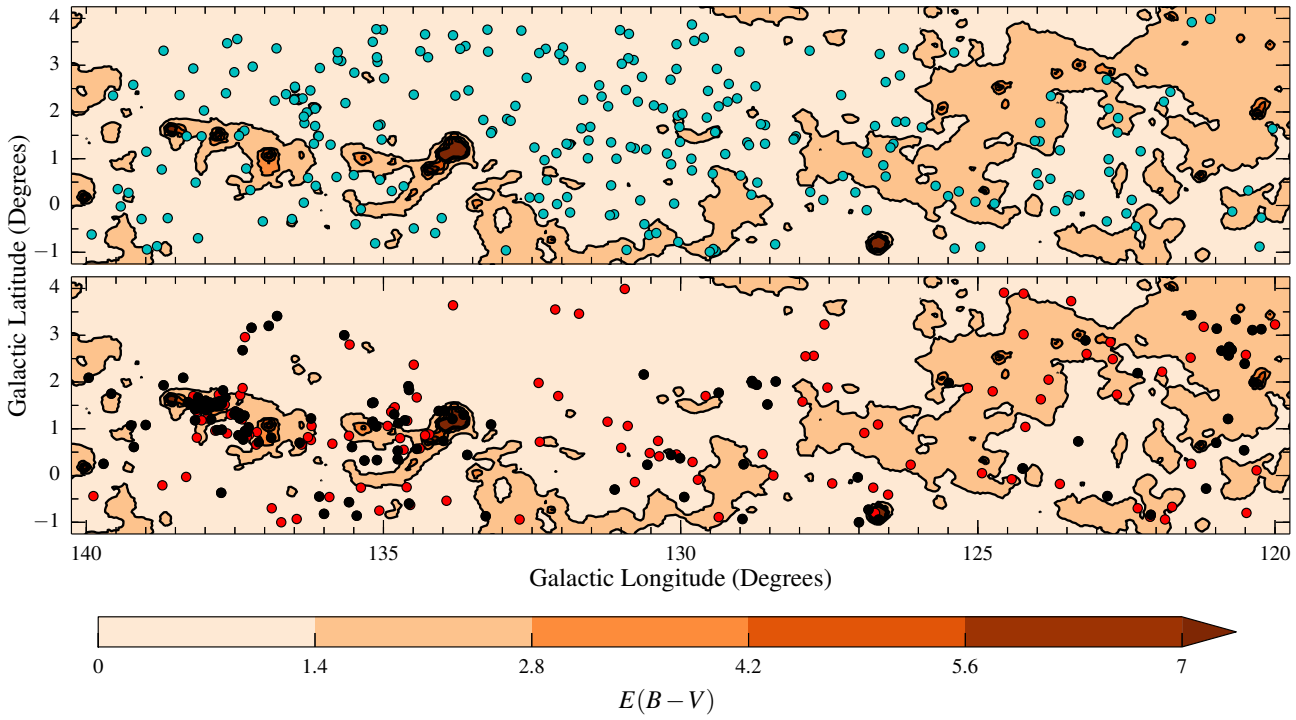

Figure 13. The spatial distributions of the 247 classical Be stars studied here (upper panel) and the 250 Hα emitters from Witham et al. (2008) (lower panel) with $16.5 < r < 18$ (red dots) and $r \geqslant 18$ (black dots) are plotted on the map of the interstellar dust extinction computed by SFD98, corrected accordingly to Schlafly et al. (2010). The extinction map is binned in 1.4 mag steps, colour coded, and cut at $E(B-V) = 7$. Comparing the two panels, we notice the higher order of clustering towards areas of higher extinction for the faintest stars from Witham et al. (2008), while fewer remain unexplored and unclassified in areas where the maximum colour excess is below 1.4 mags. In fact, we have found that our sample of classical Be stars seem not to be significantly limited by total colour excesses of up to this limit. The remaining scattered candidate emission line stars down to $r = 18$ in these locations may prove to be later-type classical Be stars.

Close to three quarters of the included stars are newly identified, with most of the rest taken from the more detailed study by paper I. Our list also includes: 3 stars (#73, 74, and 76) that were already recognised via spectroscopy as classical Be stars in the open cluster NGC 663 (see e.g. Mathew & Subramaniam 2011); 11 objects that had already been designated as Hα emitters from objective prism spectroscopy (Kohoutek & Wehmeyer 1999); 6 stars that were classified as either class II or class III SEDs by Koenig et al. (2008), according to their near- and mid-IR colours. This work moves the magnitude limit down to $r \simeq 16$ from 12–13 in the BeSS catalogue (Neiner et al. 2011).

We can already conclude that the number of classical Be stars still awaiting discovery at fainter optical magnitudes in this part of the Galactic Plane is not large. This is shown by Fig. 13 in which the spatial distributions of candidate emission line stars brighter and fainter than $r = 16.5$ (the latter being drawn from Witham et al. (2008)) are compared. The character of the faint distribution is very different from that of the bright distribution: at brighter magnitudes, the confirmed classical Be stars are distributed in a loose unclustered fashion, while the faintest candidate emission line stars ($r > 18$) are evidently much more clustered around the star-forming regions associated with high extinction. These objects will mainly be T Tauri and Herbig Ae/Be stars – leaving just a few tens of objects scattered across the general field as the more probable more mature classical Be stars in the magnitude range $16.5 < r < 18$. The job is largely done, and our enlarged list of classical Be stars – set out in the Appendices[3] – represents a significant step towards a full census of the fainter classical Be stars in this part of the Galactic Plane. It is likely that the undiscovered objects will be preferentially later type classical Be stars.

We have determined spectral types with an uncertainty ranging between 1 to 3 subtypes, depending on the S/N of the spectra available. In contrast to brighter samples, we find that later-type classical Be stars are at least as well represented as the earlier subtypes. Even with only approximate spectral sub-types, we compute reddenings that are on average good to 10 per cent. The photometric method needed to compute the corrected colour excesses, $E^{is}(B-V)$, from r, i and Hα IPHAS data only, has been shown to produce satisfactory results when compared to alternate determinations using blue data, that suffer less contamination by circumstellar disc emission.

We estimate that perhaps half of the sample, as shown by comparison with the corrected map of Schlegel et al. (1998) and the new map due to Sale et al. (2014), is compatible with heliocentric distances of 4–5 kpc or more.

The major remaining challenge is to pin down the distances to these usefully luminous objects. For this we look to the future, and the eventual release of *Gaia* parallaxes that will enable our catalogue of classical Be stars to be mapped out across the outer Galactic Plane. From the pre-launch performance data pre-

[3] Also available for download at www.iphas.org.

sented by de Bruijne (2012), the end-of-mission parallax precision for $14 < r < 16$ is expected to be in the region of 20–30 μas, or a relative error of ~ 10 per cent at distances of $\sim$5 kpc. This will be sufficient to grasp at last how the outer Galactic disc is organised.

ACKNOWLEDGEMENTS

This publication make use of spectroscopic data that were obtained at the FLWO-1.5m with FAST, which is operated by Harvard-Smithsonian Centre for Astrophysics. In particular, we would like to thank Perry Berlind and Mike Calkins for their role in obtaining most of the FLWO-1.5m/FAST data.

This paper makes use of data obtained as part of the INT Photometric Hα Survey of the Northern Galactic Plane (IPHAS, www.iphas.org) carried out at the Isaac Newton Telescope (INT). The INT is operated on the island of La Palma by the Isaac Newton Group in the Spanish Observatorio del Roque de los Muchachos of the Instituto de Astrofisica de Canarias. All IPHAS data are processed by the Cambridge Astronomical Survey Unit, at the Institute of Astronomy in Cambridge. The catalogue presented in this work was assembled at the Centre for Astrophysics Research, University of Hertfordshire, supported by a grant from the Science & Technology Facilities Council of the UK (STFC, ref ST/J001335/1).

This publication makes use of data products from the Two Micron All Sky Survey, which is a joint project of the University of Massachusetts and the Infrared Processing and Analysis Center/California Institute of Technology, funded by the National Aeronautics and Space Administration and the National Science Foundation. This publication makes use of data products from the Wide-field Infrared Survey Explorer, which is a joint project of the University of California, Los Angeles, and the Jet Propulsion Laboratory/California Institute of Technology, funded by the National Aeronautics and Space Administration.

The research leading to these results has received funding from the European Research Council under the European Union's Seventh Framework Programme (FP/2007-2013) / ERC Grant Agreement n. 320964 (WDTracer). JED, GB, and SES acknowledge support from the STFC of the United Kingdom (JED and GB ST/J001333/1, SES ST/K00106X/1). NJW is in receipt of a Fellowship funded by the Royal Astronomical Society of the United Kingdom. JF is supported by the Spanish Plan Nacional de I+D+i and FEDER under contract AYA2010-18352.

REFERENCES

Barentsen G., et al., 2014, MNRAS, 444, 3230
Carciofi A. C., Bjorkman J. E., 2006, ApJ, 639, 1081
Carciofi A. C., Bjorkman J. E., Otero S. A., Okazaki A. T., Štefl S., Rivinius T., Baade D., Haubois X., 2012, ApJ, 744, L15
Chauville J., Zorec J., Ballereau D., Morrell N., Cidale L., Garcia A., 2001, A&A, 378, 861
Collins II G. W., 1987, in Slettebak A., Snow T. P., eds, IAU Colloq. 92: Physics of Be Stars. pp 3–19
Corradi R. L. M., et al., 2008, A&A, 480, 409
Cranmer S. R., 2005, ApJ, 634, 585
Dachs J., Kiehling R., Engels D., 1988, A&A, 194, 167
Dias W. S., Alessi B. S., Moitinho A., Lépine J. R. D., 2002, A&A, 389, 871
Dougherty S. M., Waters L. B. F. M., Burki G., Cote J., Cramer N., van Kerkwijk M. H., Taylor A. R., 1994, A&A, 290, 609
Drew J. E., 1989, ApJS, 71, 267
Drew J. E., et al., 2005, MNRAS, 362, 753
Fabregat J., Torrejón J. M., 2000, A&A, 357, 451
Fabricant D., Cheimets P., Caldwell N., Geary J., 1998, PASP, 110, 79
Fitzpatrick E. L., 1999, PASP, 111, 63
Gehrz R. D., Hackwell J. A., Jones T. W., 1974, ApJ, 191, 675
Goodwin S. P., Bastian N., 2006, MNRAS, 373, 752
Gutermuth R. A., Megeath S. T., Pipher J. L., Williams J. P., Allen L. E., Myers P. C., Raines S. N., 2005, ApJ, 632, 397
Houk N., Swift C. M., Murray C. A., Penston M. J., Binney J. J., 1997, in Bonnet R. M. et al., eds, ESA Special Publication Vol. 402, Hipparcos - Venice '97. pp 279–282
Kaiser D., 1989, A&A, 222, 187
Kenyon S. J., Hartmann L., 1995, ApJS, 101, 117
Koenig X. P., Allen L. E., Gutermuth R. A., Hora J. L., Brunt C. M., Muzerolle J., 2008, ApJ, 688, 1142
Kohoutek L., Wehmeyer R., 1999, A&AS, 134, 255
Lada C. J., Adams F. C., 1992, ApJ, 393, 278
Lee U., Osaki Y., Saio H., 1991, MNRAS, 250, 432
Maciejewski G., Niedzielski A., 2007, A&A, 467, 1065
Martayan C., Frémat Y., Hubert A.-M., Floquet M., Zorec J., Neiner C., 2007, A&A, 462, 683
Massey P., Johnson K. E., Degioia-Eastwood K., 1995, ApJ, 454, 151
Mathew B., Subramaniam A., 2011, Bulletin of the Astronomical Society of India, 39, 517
Meilland A., et al., 2007, A&A, 464, 59
Mermilliod J. C., 1982, A&A, 109, 48
Meyer M. R., Calvet N., Hillenbrand L. A., 1997, AJ, 114, 288
Monet D. G., et al., 2003, AJ, 125, 984
Munari U., Sordo R., Castelli F., Zwitter T., 2005, A&A, 442, 1127
Negueruela I., Marco A., 2003, A&A, 406, 119
Neiner C., de Batz B., Cochard F., Floquet M., Mekkas A., Desnoux V., 2011, AJ, 142, 149
Oudmaijer R. D., Wheelwright H. E., Carciofi A. C., Bjorkman J. E., Bjorkman K. S., 2011, in Neiner C., Wade G., Meynet G., Peters G., eds, IAU Symposium Vol. 272, IAU Symposium. pp 418–419, doi:10.1017/S1743921311011008
Pandey A. K., Upadhyay K., Ogura K., Sagar R., Mohan V., Mito H., Bhatt H. C., Bhatt B. C., 2005, MNRAS, 358, 1290
Porter J. M., Rivinius T., 2003, PASP, 115, 1153
Raddi R., et al., 2013, MNRAS, 430, 2169
Rieke G. H., Lebofsky M. J., 1985, ApJ, 288, 618
Rivinius T., Carciofi A. C., Martayan C., 2013, A&ARv, 21, 69
Rowles J., Froebrich D., 2009, MNRAS, 395, 1640
Ruphy S., Robin A. C., Epchtein N., Copet E., Bertin E., Fouque P., Guglielmo F., 1996, A&A, 313, L21
Russeil D., Adami C., Georgelin Y. M., 2007, A&A, 470, 161
Sale S. E., et al., 2010, MNRAS, 402, 713
Sale S. E., et al., 2014, MNRAS, 443, 2907
Schlafly E. F., Finkbeiner D. P., Schlegel D. J., Jurić M., Ivezić Ž., Gibson R. R., Knapp G. R., Weaver B. A., 2010, ApJ, 725, 1175
Schlegel D. J., Finkbeiner D. P., Davis M., 1998, ApJ, 500, 525
Secchi A., 1866, Astronomische Nachrichten, 68, 63
Skrutskie M. F., et al., 2006, AJ, 131, 1163
Slettebak A., 1985, ApJS, 59, 769
Townsend R. H. D., Owocki S. P., Howarth I. D., 2004, MNRAS, 350, 189

Vallée J. P., 2014, AJ, 148, 5
Waters L. B. F., Marlborough J. M., van der Veen W. E. C., Taylor A. R., Dougherty S. M., 1991, A&A, 244, 120
Witham A. R., Knigge C., Drew J. E., Greimel R., Steeghs D., Gänsicke B. T., Groot P. J., Mampaso A., 2008, MNRAS, 384, 1277
Wright E. L., et al., 2010, AJ, 140, 1868
Zorec J., Briot D., 1991, A&A, 245, 150
Zorec J., Briot D., 1997, A&A, 318, 443
de Bruijne J. H. J., 2012, APSS, 341, 31

APPENDIX A: PHOTOMETRIC DATA

APPENDIX B: STELLAR PARAMETERS

Table A1. Optical, near-IR and mid-IR photometry of the classical Be stars in the catalogue. The columns list: the star ID number; name based on the IPHAS coordinates; Galactic coordinates (ℓ, b); IPHAS r magnitudes and $(r-i)$ and $(r-\mathrm{H}\alpha)$ colours; 2MASS J magnitudes and $(J-H)$ and $(H-K)$ colours; WISE $W1$ magnitudes and $W1-W2$, $i-W1$, and $J-W2$ colours. The tick symbols in the last two columns indicate if the object has a La Palma spectrum and/or a FLWO-1.5m/FAST spectrum. Typical uncertainties in IPHAS magnitudes and colours are 0.02 and 0.03 mag respectively.

#	Name Jhhmmss.ss+ddmmss.s	ℓ (deg)	b (deg)	r (mag)	$(r-i)$ (mag)	$(r-\mathrm{H}\alpha)$ (mag)	J (mag)	$(J-H)$ (mag)	$(H-K)$ (mag)	$W1$ (mag)	$(W1-W2)$ (mag)	$(i-W1)$ (mag)	$(J-W1)$ (mag)	LP	FF
1	J002441.72+642137.9	120.04	1.64	14.75	0.83	0.61	12.51±0.02	0.30±0.04	0.26±0.04	11.79±0.02	0.11±0.03	2.13±0.03	0.72±0.03	✓	
2	J002758.97+622906.1	120.23	−0.26	15.03	0.59	0.46	13.30±0.02	0.34±0.04	0.24±0.05	12.32±0.02	0.26±0.03	2.12±0.03	0.99±0.03		✓
3	J002843.24+615216.2	120.26	−0.88	14.38	0.48	0.42	13.16±0.02	0.17±0.04	0.20±0.05	12.58±0.03	0.18±0.04	1.32±0.03	0.58±0.03		✓
4	J002926.93+630450.2	120.45	0.32	14.07	0.40	0.36	13.11±0.02	0.12±0.04	0.18±0.04	12.87±0.03	0.01±0.04	0.80±0.03	0.24±0.03	✓	✓
5	J003210.31+623929.2	120.72	−0.13	13.39	0.47	0.51	12.33±0.02	0.22±0.04	0.15±0.04	11.37±0.02	0.32±0.03	1.55±0.03	0.96±0.03		✓
6	J003248.02+664759.6	121.09	3.99	14.41	1.02	0.85	12.11±0.02	0.55±0.03	0.36±0.03	10.45±0.02	0.29±0.03	2.93±0.03	1.66±0.03	✓	✓
7	J003559.27+664503.3	121.40	3.92	15.85	0.71	0.60	14.11±0.04	0.40±0.06	0.46±0.06	12.30±0.03	0.50±0.03	2.85±0.03	1.82±0.05	✓	✓
8	J004014.89+651644.0	121.76	2.43	14.82	0.68	0.77	12.95±0.02	0.29±0.04	0.26±0.05	12.09±0.02	0.22±0.03	2.05±0.03	0.86±0.03	✓	
9	J004121.36+650413.5	121.87	2.22	13.80	0.67	0.50	12.21±0.02	0.38±0.04	0.38±0.04	10.41±0.02	0.38±0.03	2.72±0.03	1.80±0.03		✓
10	J004517.05+640124.4	122.26	1.16	15.61	0.95	0.64	13.37±0.02	0.41±0.04	0.38±0.04	11.92±0.02	0.27±0.03	2.75±0.03	1.45±0.03	✓	✓
11	J004620.80+622503.9	122.34	−0.45	13.18	0.63	0.54	11.98±0.02	0.26±0.04	0.28±0.04	10.79±0.02	0.24±0.03	1.77±0.03	1.19±0.03		✓
12	J004651.68+625914.7	122.41	0.12	14.88	0.60	0.45	13.32±0.02	0.22±0.04	0.26±0.05	12.79±0.03	0.14±0.04	1.49±0.03	0.53±0.04	✓	✓
13	J004741.54+624203.3	122.50	−0.17	14.15	0.46	0.43	13.01±0.02	0.20±0.04	0.13±0.04	12.50±0.02	0.14±0.04	1.20±0.03	0.51±0.03		✓
14	J004842.93+644411.1	122.64	1.87	14.74	0.58	0.42	13.33±0.03	0.36±0.04	0.09±0.04	12.72±0.03	0.13±0.04	1.45±0.03	0.61±0.04		✓
15	J004850.12+642533.7	122.65	1.56	15.64	0.86	0.56	13.92±0.03	0.35±0.05	0.15±0.06	12.95±0.03	0.29±0.04	1.84±0.03	0.98±0.04		✓
16	J005011.87+635129.9	122.80	0.99	13.75	0.40	0.53	12.75±0.03	0.19±0.04	0.11±0.04	12.28±0.02	0.11±0.04	1.08±0.03	0.47±0.04		✓
17	J005011.87+633526.1	122.79	0.72	15.38	0.64	0.60	13.69±0.02	0.28±0.04	0.37±0.05	12.86±0.03	0.24±0.04	1.87±0.03	0.83±0.03	✓	✓
18	J005012.69+645621.6	122.80	2.07	14.14	0.56	0.49	12.65±0.03	0.30±0.05	0.14±0.05	11.90±0.02	0.17±0.04	1.69±0.03	0.76±0.04	✓	✓
19	J005029.22+653331.1	122.83	2.69	14.63	0.70	0.65	12.97±0.03	0.26±0.04	0.30±0.04	11.99±0.02	0.23±0.03	1.94±0.03	0.98±0.03	✓	✓
20	J005032.31+623155.5	122.83	−0.34	15.43	0.59	0.47	13.95±0.05	0.31±0.08	0.21±0.08	12.92±0.03	0.12±0.04	1.92±0.03	1.03±0.06		✓
21	J005436.84+630549.8	123.29	0.23	14.91	0.64	0.75	13.30±0.03	0.33±0.05	0.36±0.05	12.11±0.02	0.32±0.03	2.17±0.03	1.19±0.03	✓	✓
22	J005611.62+630350.5	123.47	0.20	14.40	0.55	0.46	12.95±0.02	0.18±0.03	0.18±0.03	12.47±0.02	0.08±0.03	1.38±0.03	0.47±0.03	✓	✓
23	J005619.50+625824.0	123.49	0.11	14.63	0.42	0.37	13.46±0.02	0.23±0.03	0.20±0.04	13.02±0.03	0.16±0.04	1.20±0.03	0.44±0.03	✓	✓
24	J005743.72+640235.6	123.62	1.18	14.18	0.45	0.40	13.07±0.02	0.20±0.04	0.13±0.04	12.74±0.03	0.12±0.04	0.99±0.03	0.34±0.03		✓
25	J005809.86+624412.9	123.70	−0.12	14.67	0.50	0.56	13.32±0.02	0.27±0.04	0.15±0.03	12.73±0.03	0.17±0.04	1.43±0.03	0.59±0.03		✓
26	J005859.24+632603.0	123.78	0.57	13.18	0.45	0.72	12.06±0.02	0.30±0.04	0.25±0.03	11.22±0.02	0.27±0.03	1.50±0.03	0.84±0.03		✓
27	J005926.64+651157.0	123.77	2.34	13.45	0.49	0.54	12.06±0.02	0.21±0.04	0.14±0.04	11.55±0.02	0.12±0.03	1.41±0.03	0.52±0.03		✓
28	J010045.61+631740.4	123.98	0.44	15.43	0.77	0.63	13.53±0.02	0.32±0.04	0.29±0.05	12.57±0.03	0.27±0.04	2.09±0.03	0.96±0.03	✓	✓
29	J010051.26+641327.3	123.96	1.37	13.61	0.53	0.42	12.37±0.02	0.19±0.03	0.14±0.04	11.86±0.02	0.13±0.03	1.22±0.03	0.51±0.03		✓
30	J010054.58+643729.6	123.95	1.77	13.02	0.61	0.57	11.30±0.03	0.34±0.04	0.19±0.04	10.35±0.02	0.25±0.03	2.05±0.03	0.95±0.04		✓
31	J010107.85+633227.0	124.01	0.69	13.84	0.57	0.49	12.47±0.02	0.22±0.03	0.18±0.04	11.89±0.02	0.18±0.03	1.39±0.03	0.58±0.03		✓
32	J010138.04+641349.9	124.04	1.38	13.32	0.63	0.71	11.74±0.02	0.34±0.03	0.24±0.03	10.80±0.02	0.28±0.03	1.90±0.03	0.94±0.03		✓
33	J010707.68+625117.0	124.72	0.04	14.57	0.74	0.58	12.65±0.02	0.38±0.03	0.24±0.03	11.71±0.02	0.25±0.03	2.12±0.03	0.95±0.03	✓	✓
34	J010841.17+615511.8	124.96	−0.88	13.72	0.38	0.44	12.84±0.02	0.10±0.03	0.14±0.04	12.60±0.02	0.12±0.04	0.75±0.03	0.24±0.03		✓
35	J010958.80+625229.3	125.04	0.08	14.00	0.85	0.65	12.44±0.02	0.47±0.04	0.40±0.04	10.95±0.02	0.32±0.03	2.20±0.03	1.49±0.03	✓	✓
36	J011216.30+615051.2	125.39	−0.92	13.56	0.35	0.27	12.65±0.02	0.14±0.03	0.10±0.03	12.35±0.02	−0.02±0.04	0.87±0.03	0.30±0.03		✓
37	J011234.21+630432.5	125.32	0.30	12.64	0.67	0.62	10.94±0.02	0.27±0.03	0.24±0.03	10.34±0.02	0.23±0.03	1.63±0.03	0.60±0.03		✓
38	J011402.43+625735.3	125.50	0.20	12.91	0.56	0.34	11.41±0.02	0.27±0.03	0.25±0.03						✓
39	J011543.99+660116.2	125.40	3.27	14.21	0.94	1.11	11.95±0.02	0.49±0.04	0.40±0.04	10.46±0.02	0.37±0.03	2.81±0.03	1.49±0.03	✓	✓
40	J011604.41+630926.7	125.71	0.42	14.83	0.76	0.54	12.93±0.02	0.31±0.03	0.16±0.03	11.91±0.02	0.28±0.03	2.16±0.03	1.02±0.03		✓
41	J011918.18+642233.8	125.94	1.67	13.44	0.55	0.71	12.22±0.02	0.29±0.03	0.23±0.03	11.23±0.02	0.30±0.03	1.66±0.03	0.99±0.03		✓
42	J012158.75+642813.1	126.22	1.79	14.35	0.67	0.74	12.74±0.03	0.29±0.05	0.33±0.05	11.66±0.02	0.29±0.03	2.01±0.03	1.07±0.04	✓	✓
43	J012320.11+635830.9	126.42	1.32	14.08	0.89	0.97	11.89±0.02	0.47±0.03	0.40±0.03	10.51±0.02	0.36±0.03	2.68±0.03	1.38±0.03	✓	✓
44	J012325.80+642638.7	126.37	1.79	16.32	0.67	0.57	14.60±0.03	0.27±0.05	0.11±0.08	14.10±0.03	0.03±0.06	1.56±0.04	0.51±0.04		✓
45	J012339.47+631544.2	126.55	0.62	15.04	0.80	0.61	12.97±0.02	0.45±0.03	0.29±0.03	11.90±0.02	0.21±0.03	2.33±0.03	1.07±0.03		✓
46	J012339.76+635313.0	126.47	1.24	15.07	0.82	0.75	12.96±0.02	0.41±0.03	0.35±0.03	11.99±0.02	0.26±0.03	2.26±0.03	0.96±0.03	✓	✓
47	J012358.07+652615.4	126.31	2.78	13.72	0.47	0.47	12.51±0.02	0.18±0.03	0.14±0.03	12.07±0.02	0.12±0.03	1.17±0.03	0.43±0.03		✓
48	J012405.46+660100.0	126.25	3.36	15.09	0.63	0.57	13.45±0.03	0.27±0.04	0.21±0.04	12.67±0.03	0.19±0.04	1.79±0.03	0.78±0.04	✓	✓
49	J012416.76+633011.7	126.59	0.86	13.10	0.66	0.49	11.53±0.02	0.31±0.03	0.16±0.02	10.80±0.02	0.17±0.03	1.64±0.03	0.73±0.03		✓
50	J012540.54+623025.6	126.87	−0.10	13.42	0.48	0.52	12.05±0.02	0.22±0.02	0.19±0.02	11.58±0.02	0.24±0.03	1.37±0.03	0.48±0.03	✓	✓
51	J012609.29+651618.0	126.55	2.64	14.79	0.87	0.62	12.79±0.03	0.45±0.04	0.36±0.03	11.46±0.02	0.34±0.03	2.46±0.03	1.33±0.04	✓	✓
52	J012634.69+641850.9	126.73	1.70	12.77	0.64	0.55	11.07±0.02	0.30±0.04	0.23±0.04	10.56±0.02	0.29±0.03	1.56±0.03	0.51±0.03		✓
53	J012703.28+634333.3	126.86	1.13	14.05	0.81	0.81	11.60±0.02	0.37±0.04	0.40±0.04	10.86±0.02	0.28±0.03	2.38±0.03	0.74±0.03	✓	✓
54	J012745.08+625154.3	127.06	0.28	13.46	0.45	0.58	12.04±0.02	0.24±0.03	0.21±0.04	11.25±0.02	0.27±0.03	1.76±0.03	0.80±0.03		✓
55	J012751.32+655104.2	126.65	3.24	14.51	0.71	0.75	12.77±0.02	0.37±0.04	0.28±0.04	11.67±0.02	0.27±0.03	2.14±0.03	1.10±0.03	✓	✓
56*	J013000.21+631044.6	127.27	0.63	13.76	1.02	1.09	11.33±0.02	0.56±0.03	0.53±0.04	10.32±0.02	0.50±0.03	2.42±0.03	1.01±0.03		✓
57	J013213.90+623717.2	127.60	0.12	13.32	0.54	0.43	11.96±0.02	0.22±0.04	0.17±0.03	11.37±0.02	0.19±0.03	1.42±0.03	0.59±0.03		✓
58	J013245.71+645233.3	127.30	2.36	15.42	0.76	1.02	13.31±0.03	0.47±0.04	0.40±0.05	11.68±0.02	0.32±0.03	2.99±0.03	1.63±0.04	✓	✓
59	J013422.61+624459.7	127.82	0.29	12.92	0.39	0.61	11.90±0.02	0.14±0.04	0.26±0.03	11.57±0.02	0.25±0.03	0.96±0.03	0.33±0.03		✓
60	J013739.40+613258.8	128.41	−0.83	14.31	0.63	0.50	12.73±0.03	0.31±0.04	0.16±0.04	12.26±0.02	0.06±0.03	1.42±0.03	0.47±0.04		✓
61	J013819.58+635306.0	128.06	1.48	12.98	0.61	0.91	11.50±0.03	0.31±0.04	0.34±0.03	10.34±0.02	0.29±0.03	2.03±0.03	1.16±0.03		✓
62	J013825.56+635008.5	128.08	1.43	13.96	0.53	0.47	12.70±0.03	0.24±0.04	0.11±0.04	12.01±0.02	0.16±0.03	1.42±0.03	0.69±0.04		✓
63	J013834.27+634841.3	128.10	1.41	15.28	0.65	0.56	14.16±0.03	0.17±0.05	0.15±0.07	12.80±0.03	0.26±0.04	1.82±0.04	1.36±0.04		✓
64	J013920.80+654338.7	127.83	3.31	13.64	0.61	0.47	12.20±0.02	0.24±0.04	0.18±0.04	11.75±0.02	0.11±0.03	1.28±0.03	0.45±0.03		✓
65	J014218.76+624733.5	128.71	0.49	14.56	0.60	0.50	12.90±0.03	0.30±0.04	0.23±0.04	12.08±0.02	0.17±0.03	1.88±0.03	0.82±0.03	✓	✓
66	J014238.73+633753.1	128.58	1.32	13.18	0.40	0.37	12.03±0.02	0.22±0.03	0.12±0.03	11.68±0.02	0.08±0.03	1.10±0.03	0.35±0.03		✓
67	J014244.86+623056.2	128.81	0.23	13.22	0.38	0.40	12.06±0.02	0.22±0.03	0.14±0.03	11.52±0.02	0.15±0.03	1.33±0.03	0.54±0.03		✓
68	J014322.19+640118.5	128.58	1.72	13.29	0.37	0.48	12.30±0.02	0.16±0.04	0.16±0.04	11.77±0.03	0.24±0.05	1.16±0.04	0.53±0.04		✓
69	J014401.85+640124.5	128.65	1.74	15.49	0.54	0.53	14.07±0.03	0.33±0.05	0.18±0.05						✓
70	J014458.15+633244.0	128.85	1.29	13.99	0.42	0.43	12.89±0.02	0.18±0.04	0.16±0.04	12.34±0.02	0.16±0.03	1.23±0.03	0.56±0.03	✓	✓
71	J014458.27+625245.8	128.99	0.64	13.35	0.59	0.61	11.71±0.02	0.34±0.04	0.28±0.04	10.66±0.02	0.26±0.03	2.09±0.03	1.04±0.03		✓
72	J014519.02+633559.1	128.88	1.35	13.13	0.42	0.55	12.27±0.02	0.21±0.04	0.22±0.04	11.27±0.02	0.29±0.03	1.44±0.03	1.00±0.03		✓
73	J014539.64+611259.1	129.41	−0.97	12.45	0.76	0.74	10.92±0.02	0.19±0.03	0.24±0.03	10.23±0.02	0.29±0.03	1.45±0.03	0.69±0.03		✓
74	J014602.11+611502.2	129.45	−0.93	13.75	0.55	0.71	12.39±0.03	0.26±0.05	0.25±0.04	11.68±0.03	0.33±0.04	1.51±0.04	0.71±0.04		✓
75	J014620.49+644802.5	128.74	2.55	14.41	0.48	0.43	13.25±0.03	0.23±0.04	0.17±0.04	12.66±0.03	0.21±0.04	1.27±0.03	0.59±0.04	✓	✓
76	J014624.42+611037.3	129.51	−0.99	13.36	0.45	0.34	12.22±0.02	0.17±0.04	0.14±0.04	11.93±0.03	0.02±0.04	0.99±0.03	0.30±0.03		✓
77	J014807.07+631613.2	129.25	1.10	13.54	0.60	0.69	11.92±0.02	0.25±0.03	0.38±0.03	10.77±0.04	0.32±0.05	2.18±0.04	1.15±0.04		✓
78	J014843.39+642854.4	129.05	2.29	13.74	0.45	0.49	12.66±0.02	0.24±0.04	0.15±0.04	12.04±0.02	0.14±0.03	1.25±0.03	0.62±0.03		✓
79	J014905.20+624912.3	129.46	0.68	13.60	0.81	0.68	11.49±0.02	0.34±0.04	0.48±0.04	9.97±0.02	0.26±0.03	2.82±0.03	1.51±0.03	✓	✓
80	J015001.17+642219.7	129.21	2.22	15.76	0.56	0.45	14.14±0.02	0.29±0.05	0.14±0.06	13.39±0.03	0.12±0.04	1.81±0.03	0.75±0.04		✓
81	J015022.92+652743.2	129.01	3.29	13.79	0.51	0.42	12.55±0.02	0.26±0.03	0.28±0.03	12.16±0.02	0.22±0.03	1.12±0.03	0.38±0.03		✓
82	J015030.72+634132.5	129.42	1.57	15.70	0.60	0.50	13.84±0.03	0.40±0.04	0.24±0.04	12.89±0.03	0.20±0.04	2.20±0.03	0.94±0.04		✓
83	J015037.70+644447.0	129.19	2.60	14.64	0.40	0.39	13.52±0.03	0.21±0.04	0.22±0.04	13.36±0.03	−0.07±0.05	0.88±0.03	0.17±0.04	✓	✓
84	J015105.68+611602.6	130.04	−0.78	13.71	0.50	0.37	12.50±0.03	0.24±0.04	0.18±0.03	12.02±0.02	0.09±0.03	1.19±0.03	0.48±0.03		✓
85	J015109.13+641421.8	129.36	2.12	15.71	0.57	0.48	14.27±0.03	0.33±0.05	0.08±0.06	13.80±0.03	0.16±0.05	1.33±0.04	0.47±0.04		✓

*: IPHAS photometry for these classical Be stars is not included in DR2, because the corresponding fields were D-graded in Barentsen et al. (2014). Their photometry is to be considered accurate at the level of ~ 10 per cent.

Table A1 – *continued*

#	Name Jhhmmss.ss+ddmmss.s	ℓ (deg)	b (deg)	r (mag)	$(r-i)$ (mag)	$(r-\mathrm{H}\alpha)$ (mag)	J (mag)	$(J-H)$ (mag)	$(H-K)$ (mag)	$W1$ (mag)	$(W1-W2)$ (mag)	$(i-W1)$ (mag)	$(J-W1)$ (mag)	LP	FF
86	J015213.08+624813.6	129.81	0.75	13.04	0.31	0.35	12.11 ± 0.02	0.12 ± 0.03	0.11 ± 0.03	11.70 ± 0.02	0.09 ± 0.03	1.03 ± 0.03	0.40 ± 0.03		✓
87	J015221.93+635739.6	129.56	1.88	14.29	0.56	0.61	12.79 ± 0.02	0.27 ± 0.04	0.30 ± 0.04	11.87 ± 0.02	0.29 ± 0.03	1.86 ± 0.03	0.92 ± 0.03		✓
88	J015246.27+630315.0	129.82	1.00	14.35	0.51	0.40	12.90 ± 0.02	0.25 ± 0.04	0.18 ± 0.04	12.32 ± 0.03	0.07 ± 0.04	1.52 ± 0.03	0.59 ± 0.03	✓	
89	J015307.22+650110.4	129.39	2.92	13.97	0.41	0.37	12.97 ± 0.03	0.20 ± 0.04	0.11 ± 0.04	12.47 ± 0.03	0.09 ± 0.04	1.08 ± 0.03	0.49 ± 0.04		✓
90	J015314.56+620241.5	130.11	0.04	12.89	0.39	0.31	11.88 ± 0.02	0.17 ± 0.04	0.07 ± 0.03	11.48 ± 0.02	0.06 ± 0.03	1.01 ± 0.03	0.40 ± 0.03		✓
91	J015329.19+643128.1	129.54	2.45	13.98	0.33	0.26	13.12 ± 0.02	0.11 ± 0.03	0.11 ± 0.04	12.78 ± 0.03	−0.01 ± 0.04	0.88 ± 0.03	0.35 ± 0.03		✓
92	J015427.15+612204.7	130.41	−0.59	14.38	1.08	0.84	11.55 ± 0.02	0.57 ± 0.03	0.51 ± 0.02	9.87 ± 0.02	0.38 ± 0.03	3.43 ± 0.03	1.68 ± 0.03	✓	✓
93	J015510.44+632108.5	130.01	1.36	15.85	0.50	0.41	14.46 ± 0.03	0.15 ± 0.05	0.20 ± 0.07	13.92 ± 0.04	−0.03 ± 0.06	1.42 ± 0.04	0.54 ± 0.04		✓
94	J015520.62+611752.8	130.53	−0.63	13.46	0.50	0.43	12.24 ± 0.02	0.17 ± 0.03	0.14 ± 0.02	11.62 ± 0.02	0.16 ± 0.03	1.34 ± 0.03	0.62 ± 0.03		✓
95	J015526.12+625056.4	130.16	0.88	14.34	0.55	0.61	13.11 ± 0.02	0.25 ± 0.03	0.28 ± 0.03	12.12 ± 0.03	0.31 ± 0.03	1.67 ± 0.03	0.99 ± 0.03		✓
96	J015601.25+633944.1	130.02	1.68	14.58	0.56	0.46	13.14 ± 0.02	0.18 ± 0.03	0.22 ± 0.03	12.63 ± 0.03	0.02 ± 0.04	1.39 ± 0.03	0.52 ± 0.03		✓
97	J015613.26+635623.7	129.97	1.96	14.08	0.46	0.64	12.82 ± 0.03	0.31 ± 0.04	0.33 ± 0.04					✓	✓
98	J015627.82+612939.2	130.61	−0.40	12.70	0.44	0.50	11.49 ± 0.02	0.23 ± 0.03	0.17 ± 0.03	11.26 ± 0.02	0.06 ± 0.03	1.00 ± 0.03	0.23 ± 0.03		✓
99	J015630.87+630307.5	130.23	1.11	13.28	0.27	0.51	12.52 ± 0.02	0.10 ± 0.03	0.08 ± 0.03	12.21 ± 0.03	0.15 ± 0.04	0.79 ± 0.03	0.31 ± 0.03		✓
100	J015644.71+653640.6	129.61	3.59	15.01	0.54	0.40	13.70 ± 0.02	0.14 ± 0.03	0.11 ± 0.04	13.39 ± 0.03	−0.02 ± 0.04	1.07 ± 0.03	0.31 ± 0.03		✓
101	J015645.75+635259.8	130.05	1.92	13.11	0.58	0.53	11.67 ± 0.02	0.27 ± 0.02	0.22 ± 0.02	10.88 ± 0.02	0.24 ± 0.03	1.66 ± 0.03	0.79 ± 0.03		✓
102	J015741.35+605313.7	130.91	−0.95	14.76	0.71	0.51	13.06 ± 0.02	0.31 ± 0.03	0.17 ± 0.03	12.32 ± 0.03	0.12 ± 0.04	1.72 ± 0.03	0.74 ± 0.03		✓
103	J015804.46+653020.6	129.77	3.52	13.14	0.39	0.36	12.15 ± 0.02	0.12 ± 0.03	0.17 ± 0.03	11.46 ± 0.02	0.22 ± 0.03	1.28 ± 0.03	0.69 ± 0.03		✓
104	J015809.04+615813.6	130.68	0.11	14.59	0.72	0.60	12.92 ± 0.02	0.29 ± 0.03	0.24 ± 0.03	12.35 ± 0.02	0.12 ± 0.04	1.52 ± 0.03	0.58 ± 0.03		✓
105	J015918.33+654955.8	129.81	3.87	15.19	0.55	0.54	13.80 ± 0.02	0.24 ± 0.03	0.16 ± 0.04	13.23 ± 0.03	0.19 ± 0.04	1.42 ± 0.03	0.58 ± 0.03	✓	✓
106	J015919.69+645053.4	130.07	2.92	12.78	0.34	0.53	11.88 ± 0.02	0.24 ± 0.03	0.16 ± 0.02	10.89 ± 0.02	0.25 ± 0.03	1.56 ± 0.03	0.99 ± 0.03		✓
107	J015922.56+635829.2	130.30	2.08	15.15	0.56	0.82	13.37 ± 0.02	0.45 ± 0.02	0.36 ± 0.03	12.08 ± 0.02	0.41 ± 0.03	2.51 ± 0.03	1.29 ± 0.03	✓	✓
108	J015938.99+643615.4	130.17	2.69	13.26	0.39	0.53	12.10 ± 0.02	0.27 ± 0.03	0.22 ± 0.03	11.43 ± 0.02	0.28 ± 0.03	1.45 ± 0.03	0.67 ± 0.03		✓
109	J015945.33+630314.9	130.58	1.20	14.63	0.53	0.39	13.04 ± 0.02	0.25 ± 0.04	0.12 ± 0.04	12.33 ± 0.02	0.08 ± 0.04	1.78 ± 0.03	0.71 ± 0.03		✓
110	J020037.84+652133.9	130.07	3.45	13.08	0.40	0.34	12.11 ± 0.02	0.21 ± 0.03	0.14 ± 0.03	11.79 ± 0.02	0.08 ± 0.03	0.89 ± 0.03	0.32 ± 0.03		✓
111	J020049.43+635944.0	130.45	2.14	13.91	0.84	0.57	12.39 ± 0.02	0.28 ± 0.03	0.31 ± 0.03	11.37 ± 0.02	0.33 ± 0.03	1.70 ± 0.03	1.03 ± 0.03		✓
112	J020105.33+613403.0	131.12	−0.19	14.46	0.67	0.68	12.78 ± 0.02	0.37 ± 0.03	0.31 ± 0.03	11.82 ± 0.03	0.30 ± 0.04	1.98 ± 0.04	0.96 ± 0.04		✓
113	J020121.79+630117.3	130.77	1.22	13.32	0.45	0.35	12.26 ± 0.02	0.14 ± 0.04	0.13 ± 0.04	12.05 ± 0.02	−0.06 ± 0.03	0.82 ± 0.03	0.21 ± 0.03		✓
114	J020136.00+613207.6	131.19	−0.21	13.14	0.47	0.39	11.93 ± 0.02	0.19 ± 0.04	0.15 ± 0.04	11.46 ± 0.02	0.05 ± 0.03	1.22 ± 0.03	0.47 ± 0.03		✓
115	J020203.16+630213.4	130.84	1.25	13.41	0.77	0.73	11.62 ± 0.02	0.40 ± 0.04	0.36 ± 0.04	10.43 ± 0.02	0.34 ± 0.03	2.21 ± 0.03	1.19 ± 0.03		✓
116	J020252.26+620926.0	131.17	0.43	15.21	0.60	0.57	12.91 ± 0.03	0.45 ± 0.05	0.28 ± 0.05	11.77 ± 0.02	0.09 ± 0.03	2.84 ± 0.03	1.14 ± 0.04		✓
117	J020326.01+635943.1	130.72	2.22	14.40	0.54	0.49	13.00 ± 0.03	0.22 ± 0.04	0.22 ± 0.04	11.98 ± 0.02	0.22 ± 0.03	1.88 ± 0.03	1.02 ± 0.03		✓
118	J020328.03+624333.8	131.08	1.00	13.73	0.41	0.42	12.55 ± 0.03	0.15 ± 0.04	0.14 ± 0.04	12.05 ± 0.03	0.12 ± 0.04	1.26 ± 0.03	0.50 ± 0.04		✓
119	J020407.85+643122.2	130.65	2.75	13.94	0.36	0.39	12.98 ± 0.02	0.19 ± 0.03	0.12 ± 0.04	12.47 ± 0.03	0.11 ± 0.04	1.10 ± 0.03	0.50 ± 0.03		✓
120	J020504.17+630216.1	131.17	1.35	15.07	0.57	0.41	13.68 ± 0.03	0.36 ± 0.05	0.13 ± 0.04	13.21 ± 0.03	0.02 ± 0.04	1.29 ± 0.03	0.47 ± 0.04		✓
121	J020547.47+641051.7	130.92	2.47	12.68	0.40	0.41	11.80 ± 0.02	0.17 ± 0.03	0.12 ± 0.03	11.52 ± 0.02	0.08 ± 0.03	0.76 ± 0.03	0.28 ± 0.03		✓
122	J020618.67+644945.1	130.79	3.11	14.88	0.42	0.57	13.85 ± 0.03	0.20 ± 0.05	0.15 ± 0.06	13.29 ± 0.03	0.07 ± 0.05	1.16 ± 0.04	0.55 ± 0.04		✓
123	J020707.67+612422.7	131.86	−0.15	13.28	0.39	0.37	12.27 ± 0.02	0.09 ± 0.03	0.16 ± 0.03	11.65 ± 0.02	0.19 ± 0.03	1.24 ± 0.03	0.62 ± 0.03		✓
124	J020717.23+645046.2	130.88	3.15	12.57	0.35	0.54	11.63 ± 0.02	0.18 ± 0.04	0.16 ± 0.04	11.00 ± 0.02	0.24 ± 0.03	1.22 ± 0.03	0.63 ± 0.03		✓
125	J020731.12+634520.4	131.22	2.12	14.54	0.67	0.45	12.78 ± 0.02	0.36 ± 0.04	0.18 ± 0.04	12.33 ± 0.03	0.02 ± 0.04	1.55 ± 0.03	0.45 ± 0.03		✓
126	J020734.24+623601.1	131.56	1.01	14.43	0.56	0.46	12.98 ± 0.02	0.27 ± 0.04	0.18 ± 0.04	12.36 ± 0.02	0.12 ± 0.04	1.50 ± 0.03	0.62 ± 0.03	✓	✓
127	J020753.51+644148.9	130.99	3.03	15.91	0.33	0.34	14.89 ± 0.04	0.19 ± 0.07	0.08 ± 0.12	14.36 ± 0.03	−0.42 ± 0.13	1.22 ± 0.04	0.53 ± 0.05		✓
128	J020817.76+614220.1	131.91	0.18	13.43	0.55	0.61	11.82 ± 0.02	0.32 ± 0.03	0.26 ± 0.03	10.81 ± 0.02	0.22 ± 0.03	2.07 ± 0.03	1.01 ± 0.03		✓
129	J020826.27+625745.9	131.55	1.39	14.37	0.64	0.53	12.64 ± 0.03	0.28 ± 0.04	0.24 ± 0.04	11.81 ± 0.03	0.15 ± 0.03	1.92 ± 0.03	0.83 ± 0.04		✓
130	J020837.59+652028.2	130.87	3.67	14.74	0.53	0.54	13.34 ± 0.02	0.25 ± 0.04	0.17 ± 0.04	12.59 ± 0.03	0.18 ± 0.04	1.62 ± 0.03	0.75 ± 0.03		✓
131	J020855.24+631501.1	131.52	1.68	12.72	0.54	0.61	11.60 ± 0.03	0.16 ± 0.04	0.16 ± 0.04	10.88 ± 0.02	0.14 ± 0.03	1.30 ± 0.03	0.72 ± 0.04		✓
132	J020859.72+635536.1	131.33	2.33	14.94	0.41	0.35	13.68 ± 0.03	0.19 ± 0.05	0.18 ± 0.05	13.15 ± 0.03	0.02 ± 0.05	1.38 ± 0.03	0.54 ± 0.04		✓
133	J020917.87+613045.2	132.08	0.03	13.89	0.83	0.57	11.91 ± 0.02	0.34 ± 0.04	0.23 ± 0.03	11.11 ± 0.02	0.24 ± 0.03	1.96 ± 0.03	0.80 ± 0.03		✓
134	J021000.05+640838.5	131.37	2.57	12.81	0.35	0.35	11.84 ± 0.02	0.17 ± 0.03	0.13 ± 0.03	11.28 ± 0.02	0.10 ± 0.03	1.19 ± 0.03	0.56 ± 0.03		✓
135	J021005.63+631100.3	131.67	1.65	15.98	0.51	0.39	14.64 ± 0.02	0.27 ± 0.05	0.08 ± 0.08	14.23 ± 0.03	−0.08 ± 0.07	1.24 ± 0.04	0.41 ± 0.04		✓
136	J021011.09+652230.2	131.02	3.75	13.77	0.61	0.53	12.37 ± 0.02	0.27 ± 0.03	0.14 ± 0.03	11.72 ± 0.03	0.20 ± 0.04	1.43 ± 0.03	0.65 ± 0.03		✓
137	J021036.32+611444.0	132.31	−0.18	13.09	0.50	0.42	11.66 ± 0.02	0.26 ± 0.03	0.17 ± 0.02	11.09 ± 0.02	0.13 ± 0.03	1.51 ± 0.03	0.57 ± 0.03		✓
138	J021057.06+624700.8	131.88	1.30	14.02	0.47	0.31	12.73 ± 0.02	0.29 ± 0.02	0.08 ± 0.03	12.12 ± 0.03	0.11 ± 0.03	1.44 ± 0.03	0.62 ± 0.03		✓
139	J021121.67+624707.5	131.92	1.32	15.57	0.57	0.52	13.93 ± 0.03	0.35 ± 0.05	0.25 ± 0.05					✓	✓
140	J021128.86+634604.0	131.64	2.26	13.93	0.48	0.42	12.54 ± 0.02	0.22 ± 0.03	0.15 ± 0.03	11.98 ± 0.02	0.11 ± 0.03	1.46 ± 0.03	0.56 ± 0.03		✓
141	J021159.14+615639.9	132.25	0.54	15.00	0.84	0.69	12.79 ± 0.02	0.44 ± 0.03	0.27 ± 0.03	11.97 ± 0.02	0.18 ± 0.03	2.19 ± 0.03	0.82 ± 0.03		✓
142	J021202.03+613230.4	132.38	0.16	15.41	0.83	0.59	13.27 ± 0.02	0.39 ± 0.03	0.36 ± 0.03	12.07 ± 0.02	0.32 ± 0.03	2.50 ± 0.03	1.20 ± 0.03		✓
143	J021210.42+623242.3	132.09	1.12	12.20	0.34	0.45	11.33 ± 0.02	0.13 ± 0.03	0.17 ± 0.03	10.72 ± 0.02	0.17 ± 0.03	1.14 ± 0.03	0.61 ± 0.03		✓
144	J021320.12+613003.1	132.54	0.17	12.89	0.67	0.57	11.26 ± 0.02	0.28 ± 0.02	0.23 ± 0.02	10.45 ± 0.02	0.23 ± 0.03	1.77 ± 0.03	0.82 ± 0.03		✓
145	J021325.98+622043.1	132.29	0.97	14.51	0.72	0.59	12.56 ± 0.02	0.49 ± 0.03	0.37 ± 0.03						✓
146	J021336.53+601829.1	132.94	−0.96	13.75	0.63	0.38	12.18 ± 0.02	0.26 ± 0.03	0.15 ± 0.03	11.64 ± 0.02	0.07 ± 0.03	1.49 ± 0.03	0.54 ± 0.03		✓
147	J021352.00+642520.3	131.68	2.96	15.03	0.47	0.39	13.96 ± 0.03	0.20 ± 0.05	0.19 ± 0.05	13.24 ± 0.03	0.11 ± 0.04	1.32 ± 0.03	0.72 ± 0.04		✓
148	J021532.96+623236.9	132.46	1.24	13.20	0.64	0.65	11.45 ± 0.02	0.32 ± 0.03	0.25 ± 0.02	10.21 ± 0.02	0.29 ± 0.03	2.35 ± 0.03	1.24 ± 0.03		✓
149	J021647.40+642812.9	131.97	3.11	14.59	0.52	0.46	13.28 ± 0.02	0.20 ± 0.04	0.23 ± 0.04	12.72 ± 0.02	0.18 ± 0.04	1.35 ± 0.03	0.57 ± 0.03		✓
150	J021744.41+644335.2	131.98	3.38	13.71	0.56	0.63	12.22 ± 0.02	0.29 ± 0.03	0.27 ± 0.03	11.89 ± 0.02	0.12 ± 0.03	1.25 ± 0.03	0.33 ± 0.03		✓
151	J021747.84+643419.9	132.04	3.24	14.66	0.57	0.62	13.14 ± 0.03	0.28 ± 0.04	0.27 ± 0.03						✓
152	J022009.76+643605.9	132.27	3.35	15.65	0.55	0.43	14.27 ± 0.03	0.29 ± 0.05	0.17 ± 0.07						✓
153	J022033.45+625717.4	132.86	1.81	15.71	0.71	0.85	13.90 ± 0.02	0.40 ± 0.03	0.45 ± 0.04	12.55 ± 0.03	0.38 ± 0.03	2.44 ± 0.03	1.35 ± 0.03	✓	✓
154	J022045.25+631642.8	132.78	2.13	15.02	0.52	0.49	13.85 ± 0.03	0.22 ± 0.05	0.22 ± 0.05	13.19 ± 0.03	0.14 ± 0.04	1.32 ± 0.03	0.67 ± 0.04		✓
155	J022053.65+642835.6	132.38	3.26	15.91	0.61	0.49	14.28 ± 0.03	0.31 ± 0.05	0.20 ± 0.06	13.47 ± 0.03	0.08 ± 0.05	1.83 ± 0.03	0.81 ± 0.04		✓
156	J022100.28+635435.2	132.59	2.73	13.09	0.40	0.39	12.11 ± 0.02	0.13 ± 0.04	0.13 ± 0.04	11.66 ± 0.03	0.11 ± 0.04	1.03 ± 0.03	0.45 ± 0.03		✓
157	J022107.83+625754.6	132.92	1.85	14.94	0.68	0.57	13.23 ± 0.03	0.31 ± 0.05	0.36 ± 0.05	12.09 ± 0.02	0.26 ± 0.03	2.17 ± 0.03	1.14 ± 0.04		✓
158	J022222.78+623841.9	133.17	1.59	15.17	0.58	0.43	13.54 ± 0.02	0.33 ± 0.04	0.20 ± 0.04	12.81 ± 0.03	0.13 ± 0.04	1.77 ± 0.03	0.72 ± 0.03		✓
159	J022227.73+623530.6	133.19	1.55	14.32	0.41	0.71	13.12 ± 0.03	0.23 ± 0.04	0.16 ± 0.04	12.33 ± 0.02	0.34 ± 0.03	1.58 ± 0.03	0.79 ± 0.03		✓
160	J022337.05+601602.8	134.13	−0.59	14.00	0.58	0.49	12.54 ± 0.02	0.25 ± 0.02	0.16 ± 0.03	11.34 ± 0.02	0.28 ± 0.03	2.08 ± 0.03	1.20 ± 0.03	✓	✓
161	J022343.45+603545.6	134.02	−0.27	12.94	0.66	0.44	11.24 ± 0.03	0.26 ± 0.05	0.19 ± 0.05	10.63 ± 0.03	0.11 ± 0.04	1.65 ± 0.03	0.62 ± 0.04		✓
162	J022420.68+624842.5	133.32	1.83	13.43	0.60	0.48	11.74 ± 0.02	0.32 ± 0.03	0.18 ± 0.02	11.01 ± 0.02	0.19 ± 0.03	1.82 ± 0.03	0.73 ± 0.03		✓
163	J022502.69+644947.6	132.68	3.74	13.26	0.53	0.44	11.80 ± 0.02	0.26 ± 0.03	0.19 ± 0.03	11.14 ± 0.02	0.12 ± 0.03	1.59 ± 0.03	0.66 ± 0.03		✓
164	J022636.00+601401.8	134.49	−0.49	14.50	0.96	0.99	12.13 ± 0.02	0.56 ± 0.02	0.49 ± 0.02	10.47 ± 0.02	0.42 ± 0.03	3.07 ± 0.03	1.66 ± 0.03	✓	✓
165	J022821.67+641216.0	133.24	3.29	15.84	0.61	0.49	14.16 ± 0.02	0.22 ± 0.04	0.27 ± 0.05	13.43 ± 0.03	0.12 ± 0.05	1.79 ± 0.04	0.72 ± 0.04		✓
166	J022823.86+631834.8	133.57	2.46	12.78	0.55	0.63	11.45 ± 0.02	0.28 ± 0.02	0.30 ± 0.02	11.01 ± 0.02	0.23 ± 0.03	1.21 ± 0.03	0.44 ± 0.03		✓
167	J022953.81+630742.2	133.79	2.35	14.25	0.67	0.50	12.85 ± 0.02	0.22 ± 0.03	0.15 ± 0.03	11.15 ± 0.02	0.25 ± 0.03	2.43 ± 0.03	1.70 ± 0.03	✓	✓
168	J023003.21+643829.4	133.25	3.76	15.31	0.56	0.53	13.84 ± 0.02	0.17 ± 0.04	0.24 ± 0.05	13.28 ± 0.03	0.10 ± 0.04	1.47 ± 0.03	0.56 ± 0.03		✓
169*	J023031.38+594127.1	135.14	−0.81	14.48	0.57	0.43	12.96 ± 0.02	0.31 ± 0.04	0.17 ± 0.04	12.32 ± 0.02	0.12 ± 0.03	1.60 ± 0.03	0.65 ± 0.03	✓	✓
170	J023035.11+610005.9	134.66	0.41	14.56	0.63	0.47	12.61 ± 0.02	0.42 ± 0.03	0.39 ± 0.03	11.68 ± 0.02	0.30 ± 0.03	2.25 ± 0.03	0.93 ± 0.03		✓
171	J023150.04+604952.4	134.86	0.31	13.85	0.41	0.35	12.75 ± 0.02	0.19 ± 0.03	0.12 ± 0.03	12.28 ± 0.03	0.10 ± 0.04	1.15 ± 0.03	0.47 ± 0.03		✓
172	J023202.89+641033.2	133.62	3.41	16.23	0.67	0.44	14.47 ± 0.03	0.25 ± 0.05	0.32 ± 0.06	13.78 ± 0.03	0.03 ± 0.06	1.78 ± 0.03	0.68 ± 0.04		✓

*: IPHAS photometry for these classical Be stars is not included in DR2, because the corresponding fields were D-graded in Barentsen et al. (2014). Their photometry is to be considered accurate at the level of ∼ 10 per cent.

Table A1 – *continued*

#	Name Jhhmmss.ss+ddmmss.s	ℓ (deg)	b (deg)	r (mag)	$(r-i)$ (mag)	$(r-\mathrm{H}\alpha)$ (mag)	J (mag)	$(J-H)$ (mag)	$(H-K)$ (mag)	$W1$ (mag)	$(W1-W2)$ (mag)	$(i-W1)$ (mag)	$(J-W1)$ (mag)	LP	FF
173	J023235.10+640522.7	133.71	3.35	13.53	0.76	0.76	11.62 ± 0.02	0.33 ± 0.02	0.27 ± 0.02	10.94 ± 0.02	0.31 ± 0.03	1.82 ± 0.03	0.69 ± 0.03		✓
174**	J023404.70+605914.4	135.06	0.55	12.88	0.60	0.69	11.30 ± 0.02	0.42 ± 0.03	0.51 ± 0.03	8.73 ± 0.02	1.64 ± 0.03	3.55 ± 0.03	2.57 ± 0.03	✓	✓
175	J023411.97+595634.2	135.47	−0.40	13.13	0.59	0.56	11.65 ± 0.02	0.28 ± 0.03	0.23 ± 0.03	11.27 ± 0.02	0.05 ± 0.03	1.27 ± 0.03	0.38 ± 0.03		✓
176	J023431.08+601616.5	135.38	−0.08	13.58	1.13	0.82	10.77 ± 0.02	0.55 ± 0.03	0.48 ± 0.04	9.34 ± 0.02	0.39 ± 0.03	3.12 ± 0.03	1.43 ± 0.03	✓	✓
177	J023439.79+641813.4	133.83	3.64	17.02	0.77	0.49	15.11 ± 0.04	0.28 ± 0.09	0.26 ± 0.11	14.39 ± 0.04	-0.15 ± 0.09	1.86 ± 0.04	0.72 ± 0.06		✓
178	J023536.82+625251.7	134.49	2.37	16.68	0.59	0.46	14.96 ± 0.06	0.31 ± 0.11	0.23 ± 0.13						✓
179	J023629.19+634245.8	134.25	3.17	15.61	0.64	0.60	13.92 ± 0.03	0.32 ± 0.05	0.37 ± 0.05	13.53 ± 0.03	0.11 ± 0.04	1.44 ± 0.03	0.39 ± 0.04		✓
180	J023642.66+614714.8	135.03	1.41	15.38	0.54	0.41	13.95 ± 0.05	0.33 ± 0.07	0.14 ± 0.06	13.31 ± 0.07	0.18 ± 0.10	1.53 ± 0.07	0.64 ± 0.09	✓	✓
181	J023744.52+605352.8	135.50	0.65	16.79	0.76	0.52	14.76 ± 0.04	0.27 ± 0.07	0.31 ± 0.09	14.06 ± 0.03	0.20 ± 0.06	1.97 ± 0.04	0.70 ± 0.05	✓	
182	J023753.78+620410.0	135.05	1.73	13.03	0.58	0.47	11.58 ± 0.02	0.27 ± 0.03	0.26 ± 0.03	11.97 ± 0.02	-0.02 ± 0.03	0.49 ± 0.03	-0.39 ± 0.03		✓
183	J023758.11+634635.6	134.38	3.30	13.30	0.36	0.36	12.34 ± 0.02	0.18 ± 0.03	0.07 ± 0.03	11.89 ± 0.02	0.06 ± 0.03	1.05 ± 0.03	0.45 ± 0.03		✓
184	J023809.91+620224.6	135.09	1.71	13.21	0.57	0.54	11.71 ± 0.02	0.30 ± 0.02	0.19 ± 0.02	10.96 ± 0.02	0.17 ± 0.03	1.67 ± 0.03	0.75 ± 0.03		✓
185	J023841.80+640826.3	134.30	3.66	14.05	0.64	0.44	12.38 ± 0.02	0.30 ± 0.03	0.17 ± 0.03	11.63 ± 0.02	0.16 ± 0.03	1.79 ± 0.03	0.75 ± 0.03		✓
186	J023948.17+604505.1	135.79	0.61	13.26	0.37	0.42	12.28 ± 0.02	0.21 ± 0.03	0.12 ± 0.03	11.93 ± 0.03	0.07 ± 0.04	0.96 ± 0.03	0.35 ± 0.03		✓
187	J024054.97+630009.8	134.99	2.72	15.69	0.54	0.49	14.36 ± 0.03	0.29 ± 0.05	0.21 ± 0.07	13.73 ± 0.03	0.15 ± 0.05	1.41 ± 0.04	0.63 ± 0.04	✓	✓
188	J024146.73+602532.2	136.14	0.42	14.05	0.63	0.71	12.31 ± 0.02	0.30 ± 0.03	0.25 ± 0.03	11.53 ± 0.02	0.29 ± 0.03	1.89 ± 0.03	0.78 ± 0.03	✓	✓
189	J024159.21+600106.0	136.34	0.06	14.55	0.65	0.58	12.80 ± 0.02	0.29 ± 0.02	0.21 ± 0.03	12.07 ± 0.02	0.17 ± 0.03	1.83 ± 0.03	0.73 ± 0.03	✓	✓
190	J024221.54+593716.4	136.54	−0.29	13.38	0.61	0.46	11.67 ± 0.02	0.23 ± 0.03	0.26 ± 0.03	10.74 ± 0.02	0.40 ± 0.03	2.03 ± 0.03	0.93 ± 0.03		✓
191	J024252.56+611953.9	135.89	1.30	15.74	0.64	0.73	13.95 ± 0.03	0.36 ± 0.05	0.37 ± 0.05	12.84 ± 0.03	0.33 ± 0.04	2.27 ± 0.03	1.12 ± 0.04	✓	✓
192	J024305.60+631614.7	135.10	3.07	14.55	0.55	0.61	13.27 ± 0.02	0.27 ± 0.03	0.31 ± 0.04	12.24 ± 0.02	0.27 ± 0.03	1.77 ± 0.03	1.03 ± 0.03		✓
193	J024317.68+603205.5	136.27	0.59	13.67	0.66	0.68	11.98 ± 0.03	0.32 ± 0.04	0.26 ± 0.04	10.73 ± 0.02	0.26 ± 0.03	2.28 ± 0.03	1.25 ± 0.04	✓	✓
194	J024332.05+632150.1	135.11	3.17	14.16	0.46	0.46	12.98 ± 0.02	0.21 ± 0.03	0.14 ± 0.03	12.37 ± 0.02	0.18 ± 0.03	1.34 ± 0.03	0.62 ± 0.03		✓
195	J024405.37+621448.7	135.64	2.19	15.22	0.49	0.48	13.80 ± 0.02	0.49 ± 0.03	0.49 ± 0.04	12.10 ± 0.02	0.56 ± 0.03	2.63 ± 0.03	1.69 ± 0.03	✓	✓
196	J024454.00+635608.0	135.01	3.76	15.75	0.58	0.51	14.25 ± 0.02	0.23 ± 0.05	0.22 ± 0.06	13.56 ± 0.03	0.20 ± 0.04	1.61 ± 0.03	0.69 ± 0.04		✓
197	J024504.86+612502.1	136.09	1.48	15.35	0.56	0.47	13.81 ± 0.02	0.35 ± 0.04	0.21 ± 0.04	13.01 ± 0.03	0.14 ± 0.04	1.78 ± 0.03	0.81 ± 0.03	✓	✓
198	J024506.09+611409.1	136.17	1.32	15.97	0.65	0.65	14.12 ± 0.02	0.35 ± 0.03	0.31 ± 0.04	13.07 ± 0.03	0.27 ± 0.05	2.25 ± 0.04	1.05 ± 0.04	✓	✓
199	J024509.54+612523.5	136.10	1.49	15.11	0.53	0.34	13.37 ± 0.02	0.41 ± 0.04	0.38 ± 0.04						✓
200	J024519.10+633755.1	135.18	3.50	14.04	0.55	0.62	12.74 ± 0.02	0.30 ± 0.03	0.26 ± 0.03	11.84 ± 0.02	0.26 ± 0.03	1.66 ± 0.03	0.90 ± 0.03		✓
201	J024521.28+625416.2	135.49	2.84	13.59	0.44	0.46	12.48 ± 0.02	0.19 ± 0.03	0.16 ± 0.03	11.82 ± 0.02	0.24 ± 0.03	1.33 ± 0.03	0.66 ± 0.03		✓
202	J024540.61+592151.2	137.03	−0.34	13.28	0.47	0.55	11.99 ± 0.02	0.23 ± 0.03	0.20 ± 0.03	11.59 ± 0.02	0.13 ± 0.03	1.22 ± 0.03	0.40 ± 0.03		✓
203	J024553.87+635414.7	135.12	3.77	14.21	0.68	0.53	12.48 ± 0.02	0.34 ± 0.03	0.30 ± 0.03	11.30 ± 0.03	0.29 ± 0.03	2.23 ± 0.03	1.18 ± 0.03		✓
204	J024618.12+613514.7	136.15	1.70	15.70	0.50	0.47	14.33 ± 0.03	0.27 ± 0.04	0.13 ± 0.05	13.95 ± 0.03	0.16 ± 0.06	1.25 ± 0.04	0.38 ± 0.04	✓	✓
205	J024735.56+615530.9	136.15	2.07	13.44	0.39	0.44	12.29 ± 0.02	0.23 ± 0.03	0.12 ± 0.03	11.72 ± 0.03	0.22 ± 0.04	1.33 ± 0.03	0.57 ± 0.03		✓
206	J024753.07+613405.8	136.33	1.76	14.37	0.68	0.74	12.61 ± 0.02	0.40 ± 0.03	0.27 ± 0.03	11.38 ± 0.02	0.39 ± 0.03	2.31 ± 0.03	1.24 ± 0.03		✓
207	J024758.73+630156.8	135.71	3.09	14.66	0.54	0.74	13.24 ± 0.02	0.36 ± 0.03	0.30 ± 0.03	12.13 ± 0.03	0.34 ± 0.03	1.99 ± 0.03	1.11 ± 0.03		✓
208	J024823.01+614728.1	136.29	1.99	12.91	0.38	0.48	11.72 ± 0.02	0.23 ± 0.03	0.13 ± 0.03	11.10 ± 0.02	0.16 ± 0.03	1.43 ± 0.03	0.63 ± 0.03		✓
209	J024823.69+614107.1	136.34	1.90	14.09	0.40	0.61	12.75 ± 0.02	0.29 ± 0.03	0.24 ± 0.03	11.86 ± 0.02	0.26 ± 0.03	1.82 ± 0.03	0.89 ± 0.03	✓	✓
210	J024838.04+630153.0	135.77	3.12	15.21	0.45	0.65	13.89 ± 0.03	0.23 ± 0.05	0.18 ± 0.06	13.31 ± 0.03	0.22 ± 0.04	1.45 ± 0.03	0.58 ± 0.04		✓
211	J024913.93+631042.4	135.77	3.28	13.16	0.39	0.54	12.04 ± 0.03	0.25 ± 0.05	0.27 ± 0.05						✓
212	J024928.47+595248.4	137.24	0.33	13.37	0.83	0.70	11.25 ± 0.02	0.47 ± 0.03	0.41 ± 0.03	9.94 ± 0.02	0.38 ± 0.03	2.61 ± 0.03	1.31 ± 0.03		✓
213	J024940.66+621424.8	136.23	2.46	13.24	0.33	0.45	12.36 ± 0.02	0.13 ± 0.04	0.12 ± 0.04	11.85 ± 0.02	0.15 ± 0.03	1.05 ± 0.03	0.51 ± 0.03		✓
214	J025016.65+624435.6	136.07	2.94	14.48	0.42	0.37	13.21 ± 0.02	0.24 ± 0.04	0.11 ± 0.04	12.67 ± 0.03	0.09 ± 0.04	1.39 ± 0.03	0.55 ± 0.03	✓	✓
215	J025059.12+615648.7	136.50	2.26	15.28	0.45	0.58	14.16 ± 0.03	0.21 ± 0.04	0.22 ± 0.05	13.59 ± 0.03	0.26 ± 0.05	1.24 ± 0.04	0.56 ± 0.04	✓	✓
216	J025102.21+615733.8	136.50	2.28	14.07	0.51	0.81	12.70 ± 0.02	0.30 ± 0.04	0.37 ± 0.04	11.47 ± 0.02	0.30 ± 0.03	2.08 ± 0.03	1.22 ± 0.03	✓	✓
217*	J025136.03+601557.5	137.31	0.79	15.71	0.44	0.45	14.16 ± 0.03	0.50 ± 0.05	0.37 ± 0.05	12.12 ± 0.03	0.48 ± 0.03	3.15 ± 0.03	2.04 ± 0.04		✓
218	J025200.23+621145.2	136.49	2.54	13.85	0.40	0.45	12.65 ± 0.03	0.22 ± 0.04	0.16 ± 0.04	11.96 ± 0.02	0.19 ± 0.03	1.49 ± 0.03	0.70 ± 0.03		✓
219*	J025204.14+583423.4	138.12	−0.70	12.96	0.35	0.46	11.84 ± 0.02	0.17 ± 0.03	0.17 ± 0.03	11.48 ± 0.02	0.17 ± 0.03	1.13 ± 0.03	0.35 ± 0.03		✓
220*	J025233.24+615902.2	136.64	2.38	14.82	0.43	0.36	13.60 ± 0.03	0.14 ± 0.05	0.22 ± 0.06	13.05 ± 0.03	0.09 ± 0.04	1.33 ± 0.03	0.55 ± 0.04	✓	✓
221	J025324.51+614622.9	136.83	2.24	15.46	0.59	0.58	13.79 ± 0.03	0.29 ± 0.05	0.42 ± 0.06	13.31 ± 0.03	0.12 ± 0.04	1.56 ± 0.03	0.48 ± 0.04		✓
222	J025448.83+605832.1	137.34	1.60	16.17	0.80	0.52	13.90 ± 0.03	0.41 ± 0.05	0.32 ± 0.05	12.88 ± 0.03	0.18 ± 0.05	2.49 ± 0.04	1.02 ± 0.05	✓	✓
223	J025502.38+605001.9	137.43	1.49	14.52	0.54	0.42	12.96 ± 0.02	0.33 ± 0.04	0.22 ± 0.04					✓	
224	J025610.39+580629.6	138.81	−0.87	13.81	0.62	0.25	12.30 ± 0.02	0.20 ± 0.03	0.15 ± 0.03	11.35 ± 0.02	0.29 ± 0.03	1.84 ± 0.03	0.95 ± 0.03	✓	✓
225	J025631.47+593648.4	138.16	0.49	15.01	0.70	0.74	13.26 ± 0.02	0.36 ± 0.03	0.36 ± 0.03	12.12 ± 0.02	0.32 ± 0.03	2.19 ± 0.03	1.14 ± 0.03		✓
226	J025700.47+575742.8	138.98	−0.94	14.26	0.71	0.56	12.60 ± 0.02	0.24 ± 0.03	0.15 ± 0.03	11.80 ± 0.02	0.21 ± 0.03	1.74 ± 0.03	0.80 ± 0.03	✓	✓
227	J025704.89+584311.6	138.63	−0.27	16.25	0.81	0.51	14.13 ± 0.02	0.43 ± 0.03	0.21 ± 0.04	13.26 ± 0.03	0.17 ± 0.04	2.19 ± 0.03	0.87 ± 0.04	✓	✓
228	J025737.78+624703.4	136.80	3.36	14.77	0.51	0.39	13.53 ± 0.02	0.23 ± 0.04	0.15 ± 0.05	12.92 ± 0.03	0.18 ± 0.04	1.34 ± 0.03	0.61 ± 0.03		✓
229	J025904.88+621459.5	137.20	2.97	15.59	0.39	0.34	14.48 ± 0.03	0.21 ± 0.07	0.17 ± 0.08	14.18 ± 0.03	-0.19 ± 0.08	1.02 ± 0.04	0.30 ± 0.05		✓
230	J025935.04+603207.2	138.06	1.48	13.88	0.43	0.49	12.52 ± 0.02	0.27 ± 0.04	0.21 ± 0.04	11.75 ± 0.02	0.16 ± 0.03	1.71 ± 0.03	0.77 ± 0.03		✓
231	J025959.45+582929.5	139.07	−0.29	13.31	0.63	0.49	11.69 ± 0.02	0.31 ± 0.03	0.13 ± 0.03	11.18 ± 0.02	0.07 ± 0.03	1.50 ± 0.03	0.51 ± 0.03		✓
232	J030010.27+613223.2	137.65	2.40	13.73	0.54	0.42	12.49 ± 0.02	0.11 ± 0.04	0.34 ± 0.04	11.91 ± 0.02	0.23 ± 0.03	1.28 ± 0.03	0.58 ± 0.03		✓
233	J030056.68+615940.7	137.51	2.85	13.04	0.35	0.31	12.17 ± 0.02	0.13 ± 0.03	0.10 ± 0.03	11.85 ± 0.03	-0.05 ± 0.04	0.84 ± 0.03	0.33 ± 0.03		✓
234	J030120.82+602444.9	138.31	1.48	14.38	0.55	0.48	12.83 ± 0.02	0.23 ± 0.04	0.25 ± 0.03	12.19 ± 0.03	0.14 ± 0.04	1.64 ± 0.03	0.64 ± 0.03		✓
235	J030124.02+610221.3	138.02	2.03	14.85	0.69	0.64	13.02 ± 0.02	0.32 ± 0.04	0.35 ± 0.04	11.92 ± 0.02	0.28 ± 0.03	2.24 ± 0.03	1.10 ± 0.03		✓
236	J030133.63+593518.5	138.73	0.77	14.07	0.67	0.73	12.42 ± 0.02	0.40 ± 0.03	0.33 ± 0.02	11.26 ± 0.02	0.34 ± 0.03	2.15 ± 0.03	1.17 ± 0.03		✓
237	J030317.45+583402.0	139.42	−0.02	14.57	0.80	0.61	12.51 ± 0.02	0.35 ± 0.03	0.22 ± 0.03	11.63 ± 0.02	0.19 ± 0.03	2.14 ± 0.03	0.87 ± 0.03		✓
238	J030331.33+585234.6	139.29	0.27	14.64	0.77	0.51	12.60 ± 0.03	0.37 ± 0.05	0.16 ± 0.04	11.79 ± 0.03	0.11 ± 0.04	2.09 ± 0.04	0.81 ± 0.04		✓
239	J030332.31+623856.7	137.46	3.56	14.32	0.55	0.38	12.80 ± 0.02	0.27 ± 0.04	0.17 ± 0.04	12.17 ± 0.02	0.10 ± 0.03	1.60 ± 0.03	0.63 ± 0.03		✓
240	J030422.01+574820.4	139.91	−0.62	14.40	0.65	0.54	12.91 ± 0.02	0.26 ± 0.03	0.17 ± 0.03	12.00 ± 0.02	0.25 ± 0.03	1.75 ± 0.03	0.92 ± 0.03		✓
241	J030423.32+622900.9	137.63	3.47	13.70	0.60	0.59	12.10 ± 0.02	0.31 ± 0.03	0.22 ± 0.03	11.38 ± 0.02	0.22 ± 0.03	1.72 ± 0.03	0.71 ± 0.03		✓
242	J030451.26+594758.8	138.99	1.15	15.09	0.76	0.81	13.06 ± 0.02	0.44 ± 0.05	0.38 ± 0.05	11.72 ± 0.02	0.32 ± 0.03	2.61 ± 0.03	1.34 ± 0.03		✓
243	J030501.73+585146.8	139.47	0.35	13.46	0.81	0.59	11.00 ± 0.01	0.35 ± 0.03	0.32 ± 0.03	10.75 ± 0.02	0.04 ± 0.03	1.89 ± 0.03	0.24 ± 0.03		✓
244	J030539.90+610725.6	138.43	2.36	14.47	0.81	0.73	12.21 ± 0.02	0.54 ± 0.03	0.32 ± 0.03	10.78 ± 0.02	0.28 ± 0.03	2.88 ± 0.03	1.43 ± 0.03		✓
245	J030625.00+614359.0	138.20	2.93	15.87	0.71	0.58	13.90 ± 0.03	0.40 ± 0.04	0.24 ± 0.05						✓
246	J031141.73+614847.9	138.70	3.31	15.50	0.54	0.38	14.00 ± 0.03	0.24 ± 0.04	0.18 ± 0.05	13.38 ± 0.04	0.03 ± 0.06	1.57 ± 0.04	0.61 ± 0.05		✓
247	J031208.92+605534.5	139.21	2.58	15.11	0.78	0.67	12.90 ± 0.02	0.45 ± 0.03	0.41 ± 0.03	11.58 ± 0.02	0.33 ± 0.03	2.76 ± 0.03	1.33 ± 0.03	✓	✓
248	J031333.27+603307.1	139.55	2.35	15.74	0.89	0.59	13.69 ± 0.03	0.44 ± 0.05	0.36 ± 0.05	12.34 ± 0.02	0.27 ± 0.03	2.51 ± 0.03	1.35 ± 0.04		✓

*: IPHAS photometry for these classical Be stars is not included in DR2, because the corresponding fields were D-graded in Barentsen et al. (2014). Their photometry is to be considered accurate at the level of $\sim$ 10 per cent.
**: This object is no more classified as a classical Be star but rather like a Herbig Be star.

Table B1. Stellar parameters of the 247 classical Be stars. The columns list: ID number; spectral types and S/N measured at λ4500 Å; $(r-i)$ colours corrected to zero Hα emission; intrinsic $(r-i)$ colours; colour excess; photometry $EW(\mathrm{H}\alpha)$ (typical uncertainties are in the range of 20 per cent); disc fraction; circumstellar colour excess; interstellar reddenings in the $(r-i)$ and $(B-V)$ colours; interstellar reddenings from paper I; total Galactic reddenings from SFD98 and RF09; maximum reddenings from the Sale et al. (2014) extinction-distance maps. The reddenings from SFD98 are multiplied by a correction factor of 0.86, as suggested by (Schlafly et al. 2010). The objects labelled with a "*" carry a larger photometric uncertainty, because their photometry does not meet the quality controls of DR2 (cf. Table A1 and Barentsen et al. 2014).

#	Spectral typing				$(r-i)_C$	$(r-i)_\circ$	$E(r-i)$	$EW(\mathrm{H}\alpha)$	f_D	$E^{cs}(r-i)$	$E^{is}(r-i)$	$E^{is}(B-V)$	$E^{is}(B-V)_{\mathrm{R13}}$	SFD98 ×0.86	RF09	Sale14
	R13	S/N	This work	S/N	(mag)	(mag)	(mag)	(mag)		(mag)	(mag)	(mag)	(mag)	(mag)	(mag)	(mag)
1	B5III	38			0.84	−0.08	0.92 ± 0.01	−25	0.08	0.11	0.81 ± 0.04	1.25 ± 0.06	1.36 ± 0.08	1.30	0.45	1.30
2			Mid-B	29	0.60	−0.08	0.68 ± 0.05	−16	0.05	0.07	0.61 ± 0.06	0.94 ± 0.09		1.37	0.35	1.13
3			Late-B	16	0.48	−0.04	0.52 ± 0.04	−15	0.05	0.09	0.43 ± 0.05	0.66 ± 0.08		0.81	0.27	0.79
4	B7V	66	B6	56	0.41	−0.06	0.47 ± 0.02	−11	0.04	0.07	0.40 ± 0.04	0.62 ± 0.06	0.64 ± 0.07	1.36	0.34	1.23
5			B6	44	0.48	−0.07	0.55 ± 0.01	−25	0.08	0.12	0.43 ± 0.04	0.66 ± 0.06		1.63	0.35	1.14
6	B3III	31	Early-B	38	1.06	−0.12	1.18 ± 0.02	−51	0.17	0.19	0.99 ± 0.05	1.52 ± 0.08	1.54 ± 0.08	1.57	0.74	1.59
7	A0V	26	Late-B	26	0.73	0.00	0.73 ± 0.02	−28	0.09	0.19	0.54 ± 0.05	0.83 ± 0.08	0.98 ± 0.09	1.53	0.63	1.55
8	B2V	34			0.71	−0.13	0.84 ± 0.02	−52	0.17	0.18	0.66 ± 0.04	1.02 ± 0.06	1.07 ± 0.08	1.33	0.34	1.17
9			Early-B	29	0.68	−0.13	0.81 ± 0.05	−17	0.06	0.07	0.74 ± 0.05	1.14 ± 0.08		1.32	0.53	1.15
10	B3V	24	Early-B	25	0.96	−0.12	1.08 ± 0.02	−26	0.09	0.11	0.97 ± 0.04	1.49 ± 0.06	1.34 ± 0.10	1.30	0.48	1.29
11			Mid-B	48	0.64	−0.08	0.71 ± 0.05	−23	0.08	0.11	0.60 ± 0.06	0.92 ± 0.09		1.30	0.41	1.23
12	B7V	32	Late-B	35	0.60	−0.06	0.66 ± 0.02	−14	0.05	0.08	0.58 ± 0.04	0.89 ± 0.06	0.81 ± 0.07	1.30	0.42	1.11
13			B7	34	0.46	−0.06	0.52 ± 0.02	−16	0.05	0.08	0.44 ± 0.04	0.68 ± 0.06		1.20	0.38	1.12
14			B6	48	0.58	−0.07	0.65 ± 0.01	−12	0.04	0.06	0.59 ± 0.03	0.91 ± 0.05		1.59	0.60	1.25
15			Late-B	26	0.87	−0.04	0.91 ± 0.04	−19	0.06	0.10	0.81 ± 0.06	1.25 ± 0.09		1.43	0.50	1.19
16			B5	32	0.41	−0.08	0.49 ± 0.01	−29	0.10	0.13	0.36 ± 0.04	0.55 ± 0.06		1.13	0.28	1.14
17	B3V	29	Mid-B	31	0.66	−0.12	0.78 ± 0.02	−30	0.10	0.12	0.66 ± 0.04	1.02 ± 0.06	1.07 ± 0.07	1.10	0.30	1.07
18	B5V	33	B5	66	0.56	−0.08	0.64 ± 0.01	−19	0.06	0.08	0.56 ± 0.04	0.86 ± 0.06	0.91 ± 0.08	1.38	0.62	1.27
19	B7IV	40	Mid-B	40	0.71	−0.06	0.77 ± 0.02	−34	0.11	0.17	0.60 ± 0.04	0.92 ± 0.06	1.05 ± 0.08	1.43	0.49	1.14
20			Late-B	15	0.59	−0.04	0.63 ± 0.04	−17	0.06	0.10	0.53 ± 0.05	0.82 ± 0.08		1.07	0.34	1.11
21	B2-3V	54	Mid-B	23	0.67	−0.12	0.79 ± 0.02	−51	0.17	0.18	0.61 ± 0.05	0.94 ± 0.08	0.88 ± 0.08	0.92	0.38	0.88
22	B5V	49	Late-B	34	0.56	−0.08	0.64 ± 0.01	−17	0.06	0.08	0.56 ± 0.03	0.86 ± 0.05	0.83 ± 0.09	0.99	0.23	1.06
23	B5V	81	Late-B	36	0.42	−0.08	0.50 ± 0.01	−11	0.04	0.06	0.44 ± 0.03	0.68 ± 0.05	0.64 ± 0.08	0.88	0.18	0.88
24			B5	42	0.45	−0.08	0.53 ± 0.01	−13	0.04	0.06	0.47 ± 0.03	0.72 ± 0.05		1.30	0.41	1.31
25			Late-B	23	0.51	−0.04	0.55 ± 0.04	−30	0.10	0.16	0.39 ± 0.06	0.60 ± 0.09		0.91	0.20	0.84
26			B3	26	0.47	−0.12	0.59 ± 0.02	−54	0.18	0.20	0.39 ± 0.05	0.60 ± 0.08		1.10	0.25	1.18
27			B8	45	0.49	−0.04	0.53 ± 0.02	−28	0.09	0.15	0.38 ± 0.05	0.58 ± 0.08		1.45	0.37	1.02
28	B4V	46	continuum+Balmer	8	0.78	−0.09	0.87 ± 0.02	−30	0.10	0.13	0.74 ± 0.04	1.14 ± 0.06	1.09 ± 0.08	1.18	0.34	1.09
29			Late-B	37	0.53	−0.04	0.57 ± 0.04	−13	0.04	0.07	0.50 ± 0.05	0.77 ± 0.08		1.65	0.48	1.30
30			Late-B	28	0.62	−0.04	0.66 ± 0.04	−27	0.09	0.15	0.51 ± 0.06	0.78 ± 0.09		1.66	0.57	1.42
31			Late-B	39	0.58	−0.04	0.62 ± 0.04	−19	0.06	0.10	0.52 ± 0.06	0.80 ± 0.09		1.20	0.41	1.17
32			Late-B	41	0.65	−0.04	0.69 ± 0.04	−45	0.15	0.23	0.46 ± 0.06	0.71 ± 0.09		1.65	0.48	1.25
33	B5V	58	continuum+Balmer	10	0.76	−0.08	0.83 ± 0.01	−24	0.08	0.11	0.72 ± 0.04	1.11 ± 0.06	1.06 ± 0.07	1.43	0.47	1.26
34			B6	53	0.38	−0.07	0.45 ± 0.01	−20	0.07	0.10	0.35 ± 0.04	0.54 ± 0.06		0.72	0.19	0.77
35	B3III	53	continuum+Balmer	12	0.87	−0.12	0.99 ± 0.02	−30	0.10	0.12	0.87 ± 0.04	1.34 ± 0.06	1.22 ± 0.08	1.64	0.52	1.20
36			Late-B	30	0.34	−0.04	0.38 ± 0.04	−3	0.01	0.02	0.36 ± 0.05	0.55 ± 0.08		0.99	0.24	0.84
37			B9	38	0.69	−0.02	0.71 ± 0.02	−31	0.10	0.19	0.52 ± 0.05	0.80 ± 0.08		1.68	0.56	1.45
38			B1	39	0.56	−0.15	0.71 ± 0.02	−4	0.01	0.01	0.70 ± 0.02	1.08 ± 0.03		1.51	0.71	1.43
39	B3IV	35	continuum+Balmer	16	1.03	−0.12	1.15 ± 0.02	−99	0.33	0.32	0.83 ± 0.06	1.28 ± 0.09	1.36 ± 0.08	1.26	0.61	1.12
40			Late-B	15	0.77	−0.04	0.81 ± 0.04	−19	0.06	0.10	0.71 ± 0.06	1.09 ± 0.09		1.61	0.54	1.38
41			Mid-B	42	0.57	−0.08	0.65 ± 0.05	−48	0.16	0.20	0.45 ± 0.06	0.69 ± 0.09		1.23	0.43	1.09
42	B4V	49	Mid-B	14	0.70	−0.09	0.79 ± 0.02	−47	0.16	0.19	0.60 ± 0.05	0.92 ± 0.08	0.99 ± 0.08	1.20	0.41	1.10
43	B3V	41	continuum+Balmer	26	0.95	−0.12	1.07 ± 0.02	−75	0.25	0.26	0.81 ± 0.06	1.25 ± 0.09	1.28 ± 0.08	1.63	0.71	1.23
44			Late-B	18	0.68	−0.04	0.72 ± 0.04	−25	0.08	0.14	0.58 ± 0.06	0.89 ± 0.09		1.28	0.41	1.15
45			Late-B	13	0.82	−0.04	0.86 ± 0.04	−26	0.09	0.15	0.71 ± 0.06	1.09 ± 0.09		1.69	0.65	1.45
46	B5V	27	Late-B	14	0.84	−0.08	0.92 ± 0.01	−44	0.15	0.19	0.73 ± 0.04	1.12 ± 0.06	1.33 ± 0.09	2.06	0.51	1.23
47			B7	36	0.48	−0.06	0.54 ± 0.02	−20	0.07	0.11	0.43 ± 0.04	0.66 ± 0.06		1.20	0.38	0.98
48	B6IV	27	Late-B	16	0.64	−0.07	0.71 ± 0.01	−27	0.09	0.13	0.58 ± 0.04	0.89 ± 0.06	1.10 ± 0.07	1.02	0.62	0.90
49			B3	47	0.67	−0.12	0.79 ± 0.02	−17	0.06	0.08	0.71 ± 0.03	1.09 ± 0.05		1.60	0.46	1.28
50	B5V	79	B5	39	0.48	−0.08	0.56 ± 0.01	−26	0.09	0.12	0.44 ± 0.04	0.68 ± 0.06	0.82 ± 0.07	1.02	0.37	1.27
51	B4III	39	continuum+Balmer	11	0.89	−0.09	0.98 ± 0.02	−26	0.09	0.12	0.86 ± 0.04	1.32 ± 0.06	1.29 ± 0.07	1.20	0.60	1.27
52			B3	44	0.65	−0.12	0.77 ± 0.02	−24	0.08	0.10	0.67 ± 0.04	1.03 ± 0.06		1.20	0.51	1.24
53	B3V	48	Mid-B	30	0.84	−0.12	0.96 ± 0.02	−53	0.18	0.20	0.76 ± 0.05	1.17 ± 0.08	1.31 ± 0.07	1.69	0.50	1.33
54			B3	32	0.46	−0.12	0.58 ± 0.02	−34	0.11	0.13	0.45 ± 0.04	0.69 ± 0.06		1.02	0.34	1.22
55	B7V	37	continuum+Balmer	15	0.74	−0.06	0.80 ± 0.02	−48	0.16	0.23	0.57 ± 0.05	0.88 ± 0.08	0.99 ± 0.09	1.20	0.42	1.15
56*			Early-B	24	1.10	−0.13	1.23 ± 0.15	−92	0.31	0.29	0.94 ± 0.16	1.45 ± 0.25		1.37	0.30	1.17
57			B4	37	0.54	−0.09	0.63 ± 0.02	−14	0.05	0.07	0.56 ± 0.03	0.86 ± 0.05		1.20	0.57	1.08
58	B3V	29	continuum+Balmer	18	0.83	−0.12	0.95 ± 0.02	−91	0.30	0.30	0.65 ± 0.06	1.00 ± 0.09	1.00 ± 0.09	1.18	0.37	0.96
59			B6	49	0.41	−0.07	0.48 ± 0.01	−39	0.13	0.18	0.30 ± 0.05	0.46 ± 0.08		1.14	0.30	1.05
60			Late-B	21	0.64	−0.04	0.68 ± 0.04	−19	0.06	0.10	0.58 ± 0.06	0.89 ± 0.09		1.22	0.52	1.27
61			B3	33	0.66	−0.12	0.78 ± 0.02	−76	0.25	0.26	0.52 ± 0.06	0.80 ± 0.09		0.96	0.31	0.90
62			Mid-B	23	0.54	−0.08	0.62 ± 0.05	−18	0.06	0.08	0.54 ± 0.06	0.83 ± 0.09		0.96	0.40	0.90
63			Mid-B	19	0.66	−0.08	0.74 ± 0.05	−25	0.08	0.11	0.63 ± 0.06	0.97 ± 0.09		0.97	0.40	0.90
64			B6	46	0.62	−0.07	0.69 ± 0.01	−16	0.05	0.08	0.61 ± 0.03	0.94 ± 0.05		1.05	0.48	1.23
65	B5III	42	Late-B	36	0.61	−0.08	0.69 ± 0.01	−20	0.07	0.10	0.59 ± 0.04	0.91 ± 0.06	1.05 ± 0.07	1.12	0.34	0.90
66			Late-B	34	0.41	−0.04	0.45 ± 0.04	−11	0.04	0.07	0.38 ± 0.05	0.58 ± 0.08		1.24	0.43	1.15
67			B6	31	0.38	−0.07	0.45 ± 0.01	−16	0.05	0.08	0.37 ± 0.03	0.57 ± 0.05		1.39	0.38	1.04
68			B7	34	0.37	−0.06	0.43 ± 0.02	−25	0.08	0.13	0.30 ± 0.04	0.46 ± 0.06		1.02	0.02	0.86
69			Late-B	20	0.55	−0.04	0.59 ± 0.04	−25	0.08	0.14	0.45 ± 0.06	0.69 ± 0.09		1.02	0.29	0.86
70	B7IV	66	Late-B	28	0.43	−0.06	0.49 ± 0.02	−18	0.06	0.10	0.39 ± 0.04	0.60 ± 0.06	0.77 ± 0.07	1.22	0.42	1.07
71			Early-B	24	0.61	−0.13	0.74 ± 0.05	−33	0.11	0.12	0.62 ± 0.06	0.95 ± 0.09		1.37	0.34	0.81
72			Mid-B	36	0.43	−0.08	0.51 ± 0.05	−31	0.10	0.13	0.38 ± 0.06	0.58 ± 0.09		1.17	0.41	1.05
73			B2	53	0.79	−0.13	0.92 ± 0.02	−45	0.15	0.16	0.76 ± 0.04	1.17 ± 0.06		1.80	0.38	1.36
74			B4	40	0.57	−0.09	0.66 ± 0.02	−48	0.16	0.19	0.47 ± 0.05	0.72 ± 0.08		1.97	0.05	1.36
75	B7V	44	B5	32	0.49	−0.06	0.55 ± 0.02	−15	0.05	0.08	0.47 ± 0.04	0.72 ± 0.06	0.80 ± 0.08	0.96	0.40	0.96
76			B3	43	0.45	−0.12	0.57 ± 0.02	−7	0.02	0.03	0.54 ± 0.04	0.83 ± 0.06		1.95	-0.08	1.24
77			Mid-B	29	0.62	−0.08	0.70 ± 0.05	−43	0.14	0.18	0.52 ± 0.06	0.80 ± 0.09		0.97	0.23	0.87
78			Late-B	26	0.45	−0.04	0.49 ± 0.04	−24	0.08	0.14	0.35 ± 0.06	0.54 ± 0.09		1.10	0.42	1.03
79	B3IV	46	Mid-B	31	0.83	−0.12	0.95 ± 0.02	−35	0.12	0.14	0.81 ± 0.05	1.25 ± 0.08	1.24 ± 0.07	1.50	0.36	1.05
80			Late-B	17	0.56	−0.04	0.60 ± 0.04	−15	0.05	0.09	0.51 ± 0.05	0.78 ± 0.08		1.15	0.29	0.95
81			B6	35	0.51	−0.07	0.58 ± 0.01	−14	0.05	0.08	0.50 ± 0.03	0.77 ± 0.05		0.88	0.42	0.89
82			B9	24	0.61	−0.02	0.63 ± 0.02	−20	0.07	0.14	0.49 ± 0.06	0.75 ± 0.09		1.47	0.43	0.99
83	B4V	44	Mid-B	33	0.41	−0.09	0.49 ± 0.02	−14	0.05	0.07	0.42 ± 0.03	0.65 ± 0.05	0.77 ± 0.07	0.83	0.17	0.65
84			B7	82	0.50	−0.06	0.56 ± 0.02	−8	0.03	0.05	0.51 ± 0.04	0.78 ± 0.06		1.45	0.42	1.19
85			Mid-B	22	0.58	−0.08	0.66 ± 0.05	−18	0.06	0.08	0.58 ± 0.06	0.89 ± 0.09		1.12	0.35	1.01

Table B1 – *continued*

#	Spectral typing				$(r-i)_C$	$(r-i)_\circ$	$E(r-i)$	$EW(\mathrm{H}\alpha)$	f_D	$E^{cs}(r-i)$	$E^{is}(r-i)$	$E^{is}(B-V)$	$E^{is}(B-V)_{\mathrm{R13}}$	SFD98 ×0.86	RF09	Sale14
	R13	S/N	This work	S/N	(mag)	(mag)	(mag)	(mag)		(mag)	(mag)	(mag)	(mag)	(mag)	(mag)	(mag))
86			B7	67	0.31	−0.06	0.37 ± 0.02	−12	0.04	0.07	0.30 ± 0.04	0.46 ± 0.06		1.07	0.32	0.85
87			Mid-B	17	0.58	−0.08	0.66 ± 0.05	−34	0.11	0.15	0.51 ± 0.06	0.78 ± 0.09		1.06	0.37	0.83
88	B8-9III	66			0.51	−0.03	0.54 ± 0.02	−11	0.04	0.08	0.46 ± 0.05	0.71 ± 0.08	0.86 ± 0.07	0.88	0.25	0.78
89			B5	36	0.41	−0.08	0.49 ± 0.01	−11	0.04	0.06	0.43 ± 0.03	0.66 ± 0.05		0.83	0.25	0.76
90			B6	34	0.39	−0.07	0.46 ± 0.01	−6	0.02	0.03	0.43 ± 0.03	0.66 ± 0.05		0.93	0.33	0.99
91			B7	26	0.33	−0.06	0.39 ± 0.02	−3	0.01	0.02	0.36 ± 0.03	0.55 ± 0.05		0.78	0.31	0.70
92	B4V	31	continuum+Balmer	17	1.12	−0.09	1.21 ± 0.02	−48	0.16	0.19	1.02 ± 0.05	1.57 ± 0.08	1.43 ± 0.10	1.77	0.63	1.35
93			Late-B	17	0.50	−0.04	0.54 ± 0.04	−12	0.04	0.07	0.47 ± 0.05	0.72 ± 0.08		1.11	0.28	0.80
94			B3	52	0.50	−0.12	0.62 ± 0.02	−15	0.05	0.06	0.56 ± 0.03	0.86 ± 0.05		1.43	0.52	1.24
95			B3	32	0.56	−0.12	0.68 ± 0.02	−34	0.11	0.13	0.55 ± 0.04	0.85 ± 0.06		0.91	0.30	0.68
96			Late-B	15	0.57	−0.04	0.61 ± 0.04	−17	0.06	0.10	0.51 ± 0.05	0.78 ± 0.08		1.36	0.36	1.01
97	B3V	46	B3	36	0.48	−0.12	0.60 ± 0.02	−41	0.14	0.16	0.44 ± 0.05	0.68 ± 0.08	0.64 ± 0.08	1.01	0.34	0.83
98			B1	72	0.44	−0.15	0.59 ± 0.02	−25	0.08	0.09	0.50 ± 0.04	0.77 ± 0.06		1.19	0.47	1.14
99			B4-5	75	0.28	−0.08	0.36 ± 0.02	−32	0.11	0.14	0.22 ± 0.04	0.34 ± 0.06		0.83	0.15	0.69
100			Mid-B	22	0.55	−0.08	0.63 ± 0.05	−10	0.03	0.04	0.59 ± 0.06	0.91 ± 0.09		0.93	0.24	0.85
101			B3	40	0.59	−0.12	0.71 ± 0.02	−23	0.08	0.10	0.61 ± 0.04	0.94 ± 0.06		1.40	0.25	0.88
102			Late-B	15	0.72	−0.04	0.76 ± 0.04	−17	0.06	0.10	0.66 ± 0.05	1.02 ± 0.08		2.10	0.79	1.72
103			B4	70	0.39	−0.09	0.48 ± 0.02	−11	0.04	0.05	0.43 ± 0.04	0.66 ± 0.06		0.75	0.16	0.71
104			Mid-B	23	0.73	−0.08	0.81 ± 0.05	−28	0.09	0.12	0.70 ± 0.06	1.08 ± 0.09		1.12	0.30	1.17
105	B6IV	59	Late-B	20	0.56	−0.07	0.63 ± 0.01	−26	0.09	0.13	0.50 ± 0.04	0.77 ± 0.06	0.97 ± 0.08	0.80	0.31	1.04
106			B4	81	0.34	−0.09	0.43 ± 0.02	−31	0.10	0.13	0.30 ± 0.04	0.46 ± 0.06		0.78	0.30	0.67
107	B2-3V	46	continuum+Balmer	14	0.59	−0.12	0.72 ± 0.02	−64	0.21	0.22	0.50 ± 0.05	0.77 ± 0.08	0.84 ± 0.08	0.94	0.18	0.78
108			B5	38	0.40	−0.08	0.48 ± 0.01	−30	0.10	0.13	0.34 ± 0.04	0.52 ± 0.06		0.82	0.27	0.65
109			Late-B	21	0.53	−0.04	0.57 ± 0.04	−10	0.03	0.06	0.51 ± 0.06	0.78 ± 0.09		1.12	0.32	0.89
110			Mid-B	34	0.40	−0.08	0.48 ± 0.05	−8	0.03	0.04	0.44 ± 0.06	0.68 ± 0.09		0.71	0.17	0.70
111			B3	38	0.85	−0.12	0.97 ± 0.02	−20	0.07	0.09	0.88 ± 0.04	1.35 ± 0.06		0.90	0.36	0.84
112			Mid-B	31	0.69	−0.08	0.77 ± 0.05	−39	0.13	0.17	0.60 ± 0.06	0.92 ± 0.09		1.09	0.34	0.93
113			Mid-B	27	0.45	−0.08	0.53 ± 0.05	−8	0.03	0.04	0.49 ± 0.06	0.75 ± 0.09		1.01	0.48	0.89
114			B7	66	0.47	−0.06	0.53 ± 0.02	−11	0.04	0.07	0.46 ± 0.04	0.71 ± 0.06		1.13	0.41	0.98
115			Early-B	20	0.80	−0.13	0.93 ± 0.05	−43	0.14	0.15	0.78 ± 0.06	1.20 ± 0.09		1.03	0.25	0.78
116			Mid-B	20	0.61	−0.08	0.69 ± 0.05	−27	0.09	0.12	0.57 ± 0.06	0.88 ± 0.09		1.09	0.32	1.10
117			Mid-B	31	0.55	−0.08	0.62 ± 0.05	−21	0.07	0.10	0.52 ± 0.06	0.80 ± 0.09		0.91	0.35	0.80
118			B7	52	0.42	−0.06	0.48 ± 0.02	−17	0.06	0.10	0.38 ± 0.04	0.58 ± 0.06		0.79	0.22	0.62
119			B5	32	0.36	−0.08	0.44 ± 0.01	−15	0.05	0.07	0.37 ± 0.03	0.57 ± 0.05		0.77	0.16	0.75
120			Late-B	24	0.57	−0.04	0.61 ± 0.04	−11	0.04	0.07	0.54 ± 0.05	0.83 ± 0.08		0.98	0.23	0.87
121			B1	62	0.40	−0.15	0.55 ± 0.02	−16	0.05	0.06	0.49 ± 0.03	0.75 ± 0.05		0.89	0.14	0.75
122			Mid-B	36	0.43	−0.08	0.51 ± 0.05	−34	0.11	0.15	0.36 ± 0.06	0.55 ± 0.09		0.78	0.27	0.73
123			Mid-B	43	0.39	−0.08	0.47 ± 0.05	−11	0.04	0.06	0.41 ± 0.06	0.63 ± 0.09		1.14	0.32	1.23
124			B3	48	0.36	−0.12	0.48 ± 0.02	−33	0.11	0.13	0.35 ± 0.04	0.54 ± 0.06		0.77	0.38	0.74
125			Late-B	23	0.67	−0.04	0.71 ± 0.04	−12	0.04	0.07	0.64 ± 0.05	0.98 ± 0.08		0.88	0.29	0.91
126	B6V	49	Late-B	27	0.57	−0.07	0.64 ± 0.01	−16	0.05	0.08	0.56 ± 0.03	0.86 ± 0.05	0.89 ± 0.08	1.02	0.32	0.91
127			Late-B	19	0.33	−0.04	0.37 ± 0.04	−11	0.04	0.07	0.30 ± 0.05	0.46 ± 0.08		0.73	0.17	0.74
128			B3	36	0.57	−0.12	0.69 ± 0.02	−35	0.12	0.14	0.55 ± 0.05	0.85 ± 0.08		1.23	0.58	1.21
129			A0	28	0.65	0.00	0.65 ± 0.01	−22	0.07	0.15	0.50 ± 0.06	0.77 ± 0.09		1.08	0.34	0.86
130			Late-B	19	0.54	−0.04	0.58 ± 0.04	−27	0.09	0.15	0.43 ± 0.06	0.66 ± 0.09		0.87	0.49	0.77
131			B3	41	0.55	−0.12	0.67 ± 0.02	−35	0.12	0.14	0.53 ± 0.05	0.82 ± 0.08		0.96	0.22	0.74
132			Late-B	34	0.41	−0.04	0.45 ± 0.04	−9	0.03	0.06	0.39 ± 0.06	0.60 ± 0.09		0.79	0.35	0.72
133			B9	35	0.84	−0.02	0.86 ± 0.02	−21	0.07	0.14	0.72 ± 0.05	1.11 ± 0.08		1.34	0.54	1.43
134			B8	53	0.35	−0.04	0.39 ± 0.02	−11	0.04	0.07	0.32 ± 0.04	0.49 ± 0.06		0.81	0.22	0.74
135			Late-B	13	0.51	−0.04	0.55 ± 0.04	−10	0.03	0.06	0.49 ± 0.06	0.75 ± 0.09		1.01	0.13	0.96
136			Mid-B	27	0.62	−0.08	0.70 ± 0.05	−23	0.08	0.11	0.59 ± 0.06	0.91 ± 0.09		1.06	0.40	1.10
137			B8	48	0.50	−0.04	0.54 ± 0.02	−14	0.05	0.09	0.45 ± 0.04	0.69 ± 0.06		1.23	0.58	1.23
138			B6	37	0.47	−0.07	0.54 ± 0.01	−4	0.01	0.02	0.52 ± 0.02	0.80 ± 0.03		1.54	0.40	1.13
139	B5V	22	Mid-B	25	0.58	−0.08	0.66 ± 0.02	−23	0.08	0.11	0.55 ± 0.04	0.85 ± 0.06	0.87 ± 0.15	1.38	0.54	0.99
140			B6	38	0.48	−0.07	0.55 ± 0.01	−14	0.05	0.08	0.47 ± 0.03	0.72 ± 0.05		0.87	0.37	0.73
141			Late-B	18	0.87	−0.04	0.91 ± 0.04	−35	0.12	0.19	0.72 ± 0.06	1.11 ± 0.09		1.28	0.69	1.37
142			Mid-B	13	0.85	−0.08	0.93 ± 0.05	−24	0.08	0.11	0.82 ± 0.06	1.26 ± 0.09		1.27	0.56	1.22
143			B5	65	0.34	−0.08	0.42 ± 0.01	−23	0.08	0.11	0.31 ± 0.04	0.48 ± 0.06		0.88	0.33	0.77
144			Mid-B	42	0.68	−0.08	0.76 ± 0.05	−26	0.09	0.12	0.64 ± 0.06	0.98 ± 0.09		1.29	0.51	1.22
145			Early-B	25	0.73	−0.13	0.86 ± 0.05	−26	0.09	0.10	0.76 ± 0.06	1.17 ± 0.09		1.11	0.46	1.03
146			Late-B	28	0.63	−0.04	0.67 ± 0.04	−6	0.02	0.04	0.63 ± 0.06	0.97 ± 0.09		1.81	0.74	1.46
147			B7	39	0.47	−0.06	0.53 ± 0.02	−12	0.04	0.07	0.46 ± 0.04	0.71 ± 0.06		0.86	0.29	0.83
148			Early-B	32	0.65	−0.13	0.78 ± 0.05	−37	0.12	0.13	0.65 ± 0.06	1.00 ± 0.09		0.88	0.34	0.93
149			Late-B	21	0.52	−0.04	0.56 ± 0.04	−17	0.06	0.10	0.46 ± 0.05	0.71 ± 0.08		0.91	0.38	1.00
150			B4	30	0.58	−0.09	0.67 ± 0.02	−36	0.12	0.15	0.52 ± 0.05	0.80 ± 0.08		0.97	0.46	1.10
151			Mid-B	22	0.59	−0.08	0.67 ± 0.05	−35	0.12	0.16	0.51 ± 0.07	0.78 ± 0.11		0.91	0.53	0.81
152			Late-B	22	0.56	−0.04	0.60 ± 0.04	−14	0.05	0.09	0.51 ± 0.05	0.78 ± 0.08		0.83	0.41	0.79
153	B4V	25	Mid-B	20	0.76	−0.09	0.84 ± 0.02	−62	0.21	0.24	0.60 ± 0.06	0.92 ± 0.09	0.82 ± 0.12	0.80	0.28	0.72
154			Late-B	28	0.52	−0.04	0.56 ± 0.04	−21	0.07	0.12	0.44 ± 0.06	0.68 ± 0.09		0.55	0.32	0.69
155			Late-B	18	0.61	−0.04	0.65 ± 0.04	−18	0.06	0.10	0.55 ± 0.05	0.85 ± 0.08		0.88	0.41	0.95
156			Late-B	35	0.40	−0.04	0.44 ± 0.04	−13	0.04	0.07	0.37 ± 0.05	0.57 ± 0.08		0.79	0.26	0.82
157			Mid-B	23	0.69	−0.08	0.77 ± 0.05	−25	0.08	0.11	0.66 ± 0.06	1.02 ± 0.09		0.97	0.25	0.87
158			Late-B	15	0.59	−0.04	0.63 ± 0.04	−12	0.04	0.07	0.56 ± 0.05	0.86 ± 0.08		0.70	0.41	0.85
159			B8	27	0.43	−0.04	0.47 ± 0.02	−53	0.18	0.27	0.20 ± 0.06	0.31 ± 0.09		0.71	0.44	0.93
160	B7IV	57	Late-B	17	0.58	−0.06	0.64 ± 0.02	−19	0.06	0.10	0.54 ± 0.04	0.83 ± 0.06	0.99 ± 0.07	0.82	0.56	1.24
161			B7	37	0.66	−0.06	0.72 ± 0.02	−11	0.04	0.07	0.65 ± 0.04	1.00 ± 0.06		0.62	0.61	1.41
162			Late-B	24	0.61	−0.04	0.65 ± 0.04	−17	0.06	0.10	0.55 ± 0.05	0.85 ± 0.08		0.59	0.51	0.91
163			B5	34	0.53	−0.08	0.61 ± 0.01	−15	0.05	0.07	0.54 ± 0.03	0.83 ± 0.05		0.95	0.43	0.93
164	B2V	21	continuum+Balmer	7	1.03	−0.13	1.16 ± 0.02	−76	0.25	0.24	0.92 ± 0.05	1.42 ± 0.08	1.35 ± 0.08	0.81	0.58	1.34
165			Late-B	11	0.62	−0.04	0.66 ± 0.04	−18	0.06	0.10	0.56 ± 0.05	0.86 ± 0.08		0.87	0.57	1.12
166			B3	47	0.57	−0.12	0.69 ± 0.02	−37	0.12	0.14	0.55 ± 0.05	0.85 ± 0.08		0.38	0.39	0.82
167	B2III	47	Mid-B	34	0.67	−0.13	0.80 ± 0.02	−17	0.06	0.07	0.73 ± 0.03	1.12 ± 0.05	1.02 ± 0.07	0.28	0.28	0.86
168			Late-B	23	0.57	−0.04	0.61 ± 0.04	−24	0.08	0.14	0.47 ± 0.06	0.72 ± 0.09		0.87	0.46	0.88
169*	B9V	38	Late-B	22	0.57	−0.02	0.59 ± 0.14	−13	0.04	0.08	0.51 ± 0.15	0.78 ± 0.23	0.81 ± 0.07	1.02	0.46	1.41
170			Early-B	19	0.64	−0.13	0.77 ± 0.05	−15	0.05	0.06	0.71 ± 0.05	1.09 ± 0.08		0.83	0.51	1.39

Table B1 – *continued*

#	Spectral typing				$(r-i)_c$	$(r-i)_\circ$	$E(r-i)$	$EW(\mathrm{H}\alpha)$	f_D	$E^{cs}(r-i)$	$E^{is}(r-i)$	$E^{is}(B-V)$	$E^{is}(B-V)_{\mathrm{R13}}$	SFD98 $\times 0.86$	RF09	Sale14
	R13	S/N	This work	S/N	(mag)	(mag)	(mag)	(mag)		(mag)	(mag)	(mag)	(mag)	(mag)	(mag)	(mag)
171			B4	28	0.41	−0.09	0.50 ± 0.02	−9	0.03	0.04	0.46 ± 0.04	0.71 ± 0.06		0.52	0.47	1.05
172			Late-B	25	0.67	−0.04	0.71 ± 0.04	−11	0.04	0.07	0.64 ± 0.05	0.98 ± 0.08		0.82	0.46	0.99
173			Mid-B	25	0.79	−0.08	0.87 ± 0.05	−48	0.16	0.20	0.67 ± 0.06	1.03 ± 0.09		0.85	0.45	1.05
175			B3	30	0.60	−0.12	0.72 ± 0.02	−27	0.09	0.11	0.61 ± 0.04	0.94 ± 0.06		0.91	0.59	1.35
176	B3IV	32	continuum+Balmer	18	1.17	−0.12	1.29 ± 0.02	−43	0.14	0.16	1.13 ± 0.05	1.74 ± 0.08	1.58 ± 0.07	1.70	0.74	1.57
177			Mid-B	13	0.78	−0.08	0.86 ± 0.05	−14	0.05	0.07	0.79 ± 0.06	1.22 ± 0.09		0.95	0.44	1.12
178			Late-B	12	0.60	−0.04	0.64 ± 0.04	−16	0.05	0.09	0.55 ± 0.05	0.85 ± 0.08		0.53	0.52	0.78
179			Mid-B	17	0.66	−0.08	0.73 ± 0.05	−30	0.10	0.13	0.60 ± 0.06	0.92 ± 0.09		0.82	0.39	0.85
180	B5V	50	continuum+Balmer	9	0.54	−0.08	0.62 ± 0.01	−12	0.04	0.06	0.56 ± 0.03	0.86 ± 0.05	0.78 ± 0.07	0.73	0.38	0.89
181	B8V	22			0.77	−0.04	0.81 ± 0.02	−17	0.06	0.10	0.71 ± 0.04	1.09 ± 0.06		1.06	0.41	1.13
182			Early-B	20	0.58	−0.13	0.71 ± 0.05	−17	0.06	0.07	0.64 ± 0.05	0.98 ± 0.08		0.46	0.38	0.75
183			B7	45	0.36	−0.06	0.42 ± 0.02	−12	0.04	0.07	0.35 ± 0.04	0.54 ± 0.06		0.68	0.27	0.67
184			B4	42	0.58	−0.09	0.67 ± 0.02	−25	0.08	0.10	0.57 ± 0.05	0.88 ± 0.08		0.49	0.38	0.75
185			Late-B	32	0.64	−0.04	0.68 ± 0.04	−12	0.04	0.07	0.61 ± 0.05	0.94 ± 0.08		0.87	0.55	0.94
186			Late-B	39	0.37	−0.04	0.41 ± 0.04	−18	0.06	0.10	0.31 ± 0.05	0.48 ± 0.08		0.73	0.32	0.90
187	B6V	45	continuum+Balmer	24	0.55	−0.07	0.62 ± 0.02	−20	0.07	0.10	0.52 ± 0.04	0.80 ± 0.06		0.58	0.30	0.76
188	B7V	41	Late-B	25	0.66	−0.06	0.72 ± 0.02	−44	0.15	0.22	0.50 ± 0.05	0.77 ± 0.08	1.04 ± 0.07	1.26	0.70	1.59
189	B7-8V	39	continuum+Balmer	7	0.66	−0.05	0.71 ± 0.02	−27	0.09	0.15	0.56 ± 0.04	0.86 ± 0.06		1.17	0.51	1.28
190			Late-B	28	0.61	−0.04	0.65 ± 0.04	−15	0.05	0.09	0.56 ± 0.05	0.86 ± 0.08		1.92	0.52	1.33
191	B3V	33	continuum+Balmer	13	0.67	−0.12	0.79 ± 0.02	−47	0.16	0.18	0.61 ± 0.05	0.94 ± 0.08	0.92 ± 0.08	1.08	0.39	0.94
192			Early-B	27	0.56	−0.13	0.69 ± 0.05	−34	0.11	0.12	0.57 ± 0.06	0.88 ± 0.09		0.65	0.33	0.63
193	B7V	39	Mid-B	19	0.69	−0.06	0.75 ± 0.02	−39	0.13	0.19	0.56 ± 0.05	0.86 ± 0.08	0.94 ± 0.07	1.48	0.68	1.37
194			B3	39	0.46	−0.12	0.58 ± 0.02	−19	0.06	0.08	0.50 ± 0.04	0.77 ± 0.06		0.67	0.24	0.62
195	A0III	42	Late-B	14	0.50	0.00	0.50 ± 0.01	−21	0.07	0.15	0.35 ± 0.06	0.54 ± 0.09	0.70 ± 0.07	0.62	0.26	0.67
196			Mid-B	15	0.59	−0.08	0.67 ± 0.05	−21	0.07	0.10	0.57 ± 0.06	0.88 ± 0.09		0.83	0.36	0.79
197	B7IV	40	Late-B	15	0.57	−0.06	0.63 ± 0.02	−17	0.06	0.10	0.53 ± 0.04	0.82 ± 0.06	0.87 ± 0.08	0.84	0.29	0.73
198	B3-4V	27	Late-B	16	0.67	−0.10	0.78 ± 0.02	−36	0.12	0.14	0.64 ± 0.05	0.98 ± 0.08	0.98 ± 0.08	1.05	0.38	1.14
199			Early-B	19	0.53	−0.13	0.66 ± 0.05	−5	0.02	0.02	0.64 ± 0.05	0.98 ± 0.08		0.84	0.25	0.86
200			Early-B	32	0.56	−0.13	0.69 ± 0.05	−35	0.12	0.13	0.56 ± 0.06	0.86 ± 0.09		0.78	0.26	0.79
201			Mid-B	39	0.44	−0.08	0.52 ± 0.05	−20	0.07	0.10	0.42 ± 0.06	0.65 ± 0.09		0.80	0.33	0.71
202			B3	53	0.48	−0.12	0.60 ± 0.02	−30	0.10	0.12	0.48 ± 0.04	0.74 ± 0.06		0.81	0.38	1.16
203			Mid-B	23	0.69	−0.08	0.77 ± 0.05	−21	0.07	0.10	0.67 ± 0.06	1.03 ± 0.09		0.83	0.57	0.79
204	B3V	50	Mid-B	16	0.51	−0.12	0.63 ± 0.02	−20	0.07	0.09	0.54 ± 0.04	0.83 ± 0.06	0.81 ± 0.07	0.96	0.45	0.89
205			B5	31	0.39	−0.08	0.47 ± 0.01	−20	0.07	0.10	0.37 ± 0.04	0.57 ± 0.06		2.12	0.35	0.89
206			B3	26	0.71	−0.12	0.83 ± 0.02	−47	0.16	0.18	0.65 ± 0.05	1.00 ± 0.08		0.87	0.19	0.82
207			Early-B	43	0.57	−0.13	0.70 ± 0.05	−52	0.17	0.18	0.52 ± 0.06	0.80 ± 0.09		1.25	0.29	0.61
208			B5	38	0.38	−0.08	0.46 ± 0.01	−25	0.08	0.11	0.35 ± 0.04	0.54 ± 0.06		0.87	0.49	0.76
209	B3V	43	B4	36	0.42	−0.12	0.54 ± 0.02	−40	0.13	0.15	0.39 ± 0.05	0.60 ± 0.08	0.67 ± 0.07	0.77	0.32	0.72
210			Mid-B	23	0.47	−0.08	0.55 ± 0.05	−43	0.14	0.18	0.37 ± 0.06	0.57 ± 0.09		0.99	0.23	0.61
211			Mid-B	32	0.40	−0.08	0.48 ± 0.05	−32	0.11	0.15	0.33 ± 0.06	0.51 ± 0.09		0.83	0.48	0.73
212			Early-B	29	0.85	−0.13	0.98 ± 0.05	−37	0.12	0.13	0.85 ± 0.06	1.31 ± 0.09		1.61	0.62	1.16
213			B5	40	0.34	−0.08	0.42 ± 0.01	−23	0.08	0.11	0.31 ± 0.04	0.48 ± 0.06		0.75	0.28	0.65
214	B8-9III	61	Late-B	19	0.42	−0.03	0.45 ± 0.02	−11	0.04	0.08	0.37 ± 0.05	0.57 ± 0.08	0.71 ± 0.07	0.67	0.39	0.64
215	B3-4V	35	Mid-B	20	0.46	−0.10	0.56 ± 0.02	−34	0.11	0.13	0.43 ± 0.04	0.66 ± 0.06	0.77 ± 0.08	1.07	0.30	0.95
216	B5IV	44	Mid-B	26	0.55	−0.08	0.63 ± 0.01	−65	0.22	0.26	0.37 ± 0.06	0.57 ± 0.09	0.69 ± 0.08	1.07	0.35	0.95
217*			Late-B	24	0.44	−0.04	0.48 ± 0.15	−19	0.06	0.10	0.38 ± 0.16	0.58 ± 0.25		1.26	0.67	0.97
218			B6	35	0.40	−0.07	0.47 ± 0.01	−21	0.07	0.10	0.37 ± 0.04	0.57 ± 0.06		1.63	0.31	0.62
219*			B7	45	0.35	−0.06	0.41 ± 0.14	−24	0.08	0.13	0.28 ± 0.15	0.43 ± 0.23		1.08	0.42	1.41
220*	B7V	51	Late-B	28	0.43	−0.06	0.49 ± 0.14	−9	0.03	0.05	0.44 ± 0.15	0.68 ± 0.23	0.72 ± 0.08	0.70	0.31	0.72
221			Mid-B	21	0.60	−0.08	0.68 ± 0.05	−30	0.10	0.13	0.55 ± 0.06	0.85 ± 0.09		0.60	0.42	0.87
222	B6V	25	Late-B	19	0.81	−0.07	0.88 ± 0.02	−16	0.05	0.08	0.80 ± 0.03	1.23 ± 0.05	1.20 ± 0.10	1.39	0.68	1.38
223	B7V	55			0.54	−0.06	0.60 ± 0.02	−13	0.04	0.07	0.53 ± 0.04	0.82 ± 0.06		1.44	0.48	1.08
224	B5V	45	Mid-B	24	0.60	−0.08	0.68 ± 0.14	−12	0.04	0.06	0.62 ± 0.15	0.95 ± 0.23	0.93 ± 0.07	1.33	0.72	1.39
225			Mid-B	20	0.73	−0.08	0.81 ± 0.05	−46	0.15	0.19	0.62 ± 0.06	0.95 ± 0.09		0.65	0.44	0.99
226	B4V	30	Mid-B	27	0.73	−0.09	0.82 ± 0.02	−24	0.08	0.10	0.72 ± 0.05	1.11 ± 0.08	1.06 ± 0.08	1.48	0.65	1.49
227	B5V	33	Mid-B	15	0.81	−0.08	0.89 ± 0.02	−14	0.05	0.07	0.82 ± 0.03	1.26 ± 0.05	1.22 ± 0.09	1.14	0.55	1.16
228			Late-B	20	0.52	−0.04	0.56 ± 0.04	−10	0.03	0.06	0.50 ± 0.06	0.77 ± 0.09		0.77	0.35	0.87
229			Late-B	18	0.39	−0.04	0.43 ± 0.04	−9	0.03	0.06	0.37 ± 0.06	0.57 ± 0.09		0.65	0.38	0.71
230			Late-B	26	0.43	−0.04	0.47 ± 0.04	−24	0.08	0.14	0.33 ± 0.06	0.51 ± 0.09		1.38	0.90	1.00
231			Late-B	27	0.64	−0.04	0.68 ± 0.04	−18	0.06	0.10	0.58 ± 0.05	0.89 ± 0.08		1.29	0.49	1.27
232			Early-B	44	0.54	−0.13	0.67 ± 0.05	−12	0.04	0.05	0.62 ± 0.05	0.95 ± 0.08		0.54	0.36	0.93
233			Mid-B	48	0.35	−0.08	0.43 ± 0.05	−7	0.02	0.03	0.40 ± 0.06	0.62 ± 0.09		0.62	0.30	0.81
234			Mid-B	16	0.55	−0.08	0.63 ± 0.05	−19	0.06	0.08	0.55 ± 0.06	0.85 ± 0.09		2.74	0.74	1.00
235			Mid-B	30	0.70	−0.08	0.78 ± 0.05	−33	0.11	0.15	0.63 ± 0.06	0.97 ± 0.09		0.97	0.64	1.05
236			B3	36	0.69	−0.12	0.81 ± 0.02	−47	0.16	0.18	0.63 ± 0.05	0.97 ± 0.08		0.86	0.52	1.00
237			Late-B	25	0.81	−0.04	0.85 ± 0.04	−27	0.09	0.15	0.70 ± 0.06	1.08 ± 0.09		1.14	0.59	1.24
238			Mid-B	23	0.78	−0.08	0.86 ± 0.05	−16	0.05	0.07	0.79 ± 0.06	1.22 ± 0.09		1.32	0.67	1.37
239			Late-B	31	0.55	−0.04	0.59 ± 0.04	−8	0.03	0.06	0.53 ± 0.06	0.82 ± 0.09		0.90	0.46	0.77
240			Late-B	27	0.66	−0.04	0.70 ± 0.04	−23	0.08	0.14	0.56 ± 0.06	0.86 ± 0.09		1.08	0.52	1.50
241			Mid-B	31	0.61	−0.08	0.69 ± 0.05	−30	0.10	0.13	0.56 ± 0.06	0.86 ± 0.09		0.91	0.42	0.87
242			Early-B	15	0.80	−0.13	0.93 ± 0.05	−55	0.18	0.19	0.74 ± 0.06	1.14 ± 0.09		1.14	0.57	1.09
243			Mid-B	30	0.83	−0.08	0.91 ± 0.05	−24	0.08	0.11	0.80 ± 0.06	1.23 ± 0.09		1.18	0.62	1.13
244			Mid-B	23	0.84	−0.08	0.92 ± 0.05	−42	0.14	0.18	0.74 ± 0.06	1.14 ± 0.09		0.93	0.98	1.39
245			Late-B	11	0.73	−0.04	0.77 ± 0.04	−25	0.08	0.14	0.63 ± 0.06	0.97 ± 0.09		0.81	0.31	0.98
246			Late-B	24	0.55	−0.04	0.59 ± 0.04	−9	0.03	0.06	0.53 ± 0.06	0.82 ± 0.09		0.84	0.33	0.73
247	B4V	35	Early-B	11	0.80	−0.09	0.89 ± 0.02	−34	0.11	0.14	0.74 ± 0.04	1.14 ± 0.06	1.11 ± 0.11	1.30	0.72	1.30
248			Late-B	14	0.90	−0.04	0.94 ± 0.04	−22	0.07	0.12	0.82 ± 0.06	1.26 ± 0.09		1.35	0.66	1.23